In situ Sr isotope analysis of mantle carbonates: Constraints on the evolution and sources of metasomatic carbon-bearing fluids in a paleo-collisional setting

Published Version:

In situ Sr isotope analysis of mantle carbonates: Constraints on the evolution and sources of metasomatic carbon-bearing fluids in a paleo-collisional setting / Consuma G.; Braga R.; Giovanardi T.; Bersani D.; Konzett J.; Lugli F.; Mazzucchelli M.; Tropper P.. - In: LITHOS. - ISSN 0024-4937. - ELETTRONICO. - 354-355:(2020), pp. 105334.1-105334.15. [10.1016/j.lithos.2019.105334]

Availability:

Published:

DOI: http://doi.org/10.1016/j.lithos.2019.105334

Terms of use:

Giulia Consuma, Roberto Braga, Tommaso Giovanardi, Danilo Bersani, Jürgen Konzett, Federico Lugli, Maurizio Mazzucchelli, Peter Tropper (2020). In situ Sr isotope analysis of mantle carbonates: Constraints on the evolution and sources of metasomatic carbon-bearing fluids in a paleo-collisional setting, Lithos, 354–355

The final published version is available online at ***https://dx.doi.org/10.1016/j.lithos.2019.105334***

In situ Sr isotope analysis of mantle carbonates: constraints on the evolution and sources of metasomatic carbon-bearing fluids in a paleo-collisional setting

Giulia Consuma[a], Roberto Braga[a,*], Tommaso Giovanardi[b], Danilo Bersani[c], Jürgen Konzett[d], Federico Lugli[e], Maurizio Mazzucchelli[b], Peter Tropper[d]

[a] Department of Biological, Geological and Environmental Sciences, University of Bologna, Piazza di Porta San Donato 1, 40126 Bologna, Italy
[b] Department of Chemical and Geological Sciences, University of Modena and Reggio Emilia, Via Campi 103, 41125 Modena, Italy
[c] Department of Mathematical, Physical and Computer Sciences, University of Parma, Parco Area delle Scienze 7/A, 43124, Parma, Italy
[d]Institute of Mineralogy and Petrology, University of Innsbruck, Innrain52, 6020 Innsbruck, Austria
[e]Department of Cultural Heritage, University of Bologna, Via degli Ariani 1, 48100 Ravenna, Italy

*Corresponding author: r.braga@unibo.it (Roberto Braga)

ABSTRACT

Carbonate-bearing wedge peridotites attest the mobilization of carbon (C) by slab fluids/melts circulating in a subduction setting. In general, COH fluids are thought to derive from the dehydration/partial melting of the crustal portions of slabs, especially during the exhumation of crust-mantle mélanges along continental subduction channels. In this study we combined textural observations with *in-situ* Sr isotope analyses of mantle carbonates occurring in different microstructural sites to test whether the fluids responsible for the carbonation of a mantle wedge derived from the subducted continental crust or not. We focus on the Ulten Zone peridotites (Eastern Italian Alps) associated with high-grade felsic rocks, where carbonates occur mainly as dolomite and minor magnesite and calcite. Analyses by a laser ablation system coupled to a Neptune MC-ICP-MS on peridotites representing different episodes of a complex metasomatic history, indicate that Sr isotopic variations can be linked to the different microstructural positions of carbonates. The C-metasomatism of UZ peridotites can be outlined in two stages. The first stage is the *HP*-carbonation at peak (eclogite-facies) conditions, with formation of interstitial matrix dolomite in textural equilibrium with hornblende to pargasite amphibole and Cl-apatite. This dolomite exhibits relatively unradiogenic $^{87}\text{Sr}/^{86}\text{Sr}$ present day values of 0.70487±0.00010, requiring different sources with respect to the associated migmatites and the overhanging mantle wedge. Carbonation continued during exhumation, with local injection of C-rich fluids forming dolomite veins in association with tremolite and chlorite. The dolomite vein shows a wide range of $^{87}\text{Sr}/^{86}\text{Sr}$ (0.7036-0.7083), reflecting both the primary composition of carbonates and the consequent interaction with crustal fluids as expected in a crust-mantle mélange. The second stage is C-remobilization during the final exhumation by dolomite dissolution and precipitation of brucite intergrowths with calcite, that exhibits a quite similar Sr composition of the precursor dolomite.

The mantle wedge is therefore capable to store carbonates representing a complex metasomatic evolution from eclogite-facies conditions to very shallow structural levels. Fluids released from subducting slabs of continental lithosphere might be responsible for the crystallization, in the overlying ultramafic rocks, of metasomatic minerals such as amphibole, phlogopite and zircon, but their role on the carbonation of mantle wedge is most likely overestimated. The combination of geochemical, isotopic and textural evidence suggests the contribution of a distinct source of C-bearing fluids for included and interstitial dolomite, which could be related to depleted mantle wedge sources and/or trondhjemitic igneous activity. Differently, residual COH-fluids released by the associated stromatic gneisses and orthogneisses acted during the end of exhumation, providing the highest Sr isotope values for the dolomite veins.

Keywords: Carbon Cycle; peridotite; mantle-wedge; In situ Sr isotope; metasomatism; Ulten Zone

1 Introduction

At convergent plate boundaries, the interface between subducting slab and overhanging mantle wedge represents a complex region, where a mix of slab- and wedge-derived lithologies plays a key role in the surface-to-mantle volatiles budget on Earth (Bebout and Penniston-Dorland, 2016). In this tectonic setting, the subduction of carbon (C) stored in organic matter and carbonate minerals is partly returned to the surface by slab fluids (Manning, 2014). The occurrence of hydrous and carbonated phases, and the enrichment in incompatible elements of the lithospheric mantle wedge above a subducting slab, testify the fluid-mediated large-scale cycling of elements. The C transfer among different reservoirs is usually related to fluids or melts expelled from the crustal portion of the subducted oceanic lithosphere (carbonated serpentinite, altered crust and sediments). However, many of the studied mantle wedge peridotites are now exposed within variable migmatized felsic gneisses, as a result of continental collision (Brueckner and Medaris, 2000; Zheng, 2012 and references therein). Accordingly, several studies highlight the importance of subducted continental crust as source of metasomatic C-bearing fluids/hydrous melts reacting and enriching the overhanging mantle wedge (Zanetti et al., 1999; Zheng, 2009; Hermann et al., 2013). An appropriate identification of the C sources during interactions between mantle wedge and subducted continental lithosphere is therefore essential in order to develop a quantitative understanding of the global C flux.

In this study we take advantage of the wealth of data already available on the multiple metasomatic history of the Ulten Zone (UZ) peridotite (northern Italy) to illustrate the formation and the dissolution-reprecipitation of carbonates at relatively shallow (P < 3 GPa) and cold (T < 850°C) conditions. The UZ peridotites record the transition from mantle wedge, coarse-grained, spinel-peridotite to high-pressure, fine-grained, garnet-bearing amphibole-peridotite and, finally to low-P, low-T serpentinized peridotites (Förster et al., 2017; Ionov et al., 2017; Gudelius et al., 2018). Therefore, these rocks offer the opportunity to investigate fluid-driven carbonation at different P-T conditions, along the complex metasomatic evolution of a paleo-mantle wedge involved in continental collision. We combined microstructural observations, major elements compositions, micro-Raman analyses of carbonates and associated minerals, with in situ $^{87}Sr/^{86}Sr$ isotopic composition of carbonates as a tracer for investigating the potential sources of C-bearing fluids. The choice of using elemental Sr and $^{87}Sr/^{86}Sr$ ratio to shed more light on C-metasomatism is based on the fact that: (i) it is relatively abundant in the carbonates structure due to its easy substitution with Ca^{2+}; (ii) the partition of Rb into the carbonate crystal structure is hampered because of its large ionic size, and we therefore assume that carbonates may inherit the Sr isotopic composition of C-bearing fluids at the time of their formation and their release from the sources (Dickin, 2018 and references therein); (iii) its concentration and isotopic composition may provide information about fluid sources, elements partitioning, isotopic mixing behavior and extent of fluid-rock interaction (Banner, 1995). *In situ* approaches applied to carbonates can therefore provide the spatial resolution to better constrain the carbon-volatile-element mobilization in a crust-mantle interface and the element exchange at grain-scale.

2.Geology and petrology of the Ulten Zone

In the Ulten Valley and Non Valley (Trentino-Alto Adige, Italy), the Ulten Zone is a tectono-metamorphic complex belonging to the Tonale Nappe, Upper Austroalpine domain of the Eastern Alps (Fig.1). The Tonale Nappe forms a SW-NE oriented narrow belt of Variscan metamorphic rocks, bounded by Alpine faults such as the Tonale and Giudicarie lines to the South and the Peio Line to the North (Müller et al., 2001). The UZ consists of strongly foliated garnet-kyanite gneisses and migmatites enclosing lenses of peridotites and pyroxenites (Obata and Morten, 1987). The main metamorphic overprint is Variscan in age whereas the evidences of a weak Eo-Alpine overprint mostly occur along the main tectonic lines (Godard et al., 1996).

Considering the different grain size and metamorphic assemblage, Obata and Morten (1987) classified the UZ peridotites as ranging from less deformed coarse-grained spinel peridotites to foliated fine-grained garnet-amphibole/chlorite-amphibole peridotites: the latter are interpreted as deformed and recrystallized derivatives of the former.

The UZ petrology and metasomatic evolution is the subject of several studies well summarized in Scambelluri et al. (2010) and the sketch of Figure 2 contains the main features of an otherwise complex sequence of events. In stage 1 (Fig. 2), coarse-grained peridotites made of olivine + enstatite + diopside + Cr-Al spinel with protogranular texture (Obata and Morten, 1987) were percolated by hydrous basic melts from deeper lithospheric mantle before the Variscan orogeny, leading to LREE and LILE enrichment at spinel facies conditions (1200°C and 1.3-1.6 GPa; Nimis and Morten, 2000).

During stage 2, related to the Variscan subduction, corner flow dragged the coarse-peridotites close to the slab-wedge interface and caused the transition to porphyroclastic to fine-grained equigranular peridotites. The porphyroclastic type shows garnet corona around spinel and the occurrence of pale green amphibole in the peridotite matrix (Obata and Morten, 1987). However, well preserved spinel-facies coarse-peridotites are fairly rare in the field and the transitional evolution of the different lithotypes is still somewhat enigmatic.

Fine-grained peridotites show different mineral assemblages, mainly distinguished by the presence/absence of garnet and clinopyroxene, ranging from olivine + orthopyroxene + clinopyroxene + garnet + Ca-amphibole ± spinel to olivine + orthopyroxene + Ca-amphibole + chlorite (Obata and Morten, 1987). Phlogopite, apatite, dolomite and rare dissakisite-(La) are accessories (Tumiati et al., 2007). Fine-grained peridotites resulted from mylonitization and hydration of the coarse-peridotites that interacted with slab-derived fluids during the Variscan continental collision. The metamorphic peak was estimated around 850°C and 2.0-2.5 GPa in eclogite-facies conditions (Nimis and Morten, 2000; Braga and Sapienza, 2007), concomitant to a widespread crystallization of LILE- and LREE-rich amphibole, in textural equilibrium with garnet (Scambelluri et al., 2006). The timing of tectonic emplacement into the crust is still uncertain: garnet-whole rock and garnet-clinopyroxene isochrones Sm-Nd ages of Tumiati et al. (2003) suggest that garnet-facies equilibration and metasomatism in peridotite, and country rocks migmatization occurred at the same time, about 340-330 Ma. This argument supported the notion that the tectonic insertion of peridotite into the subducted continental crust occurred at peak conditions (Tumiati et al., 2003). Conversely, Scambelluri et al. (2006) stressed that the incorporation of mantle wedge peridotites into the crustal slab to form a crust-mantle mélange likely occurred shortly after the metamorphic peak.

Stage 3 (Fig. 2) represents the retrograde evolution of the crust-mantle association, recorded by (i) kelyphitic coronas around garnet in fine-grained garnet-amphibole peridotites (Godard and Martin, 2000) and (ii) the occurrence of fine-grained spinel/chlorite-amphibole peridotite, interpreted as retrograde derivates from garnet-peridotites (Obata and Morten, 1987; Braga and Sapienza 2007; Marocchi et al., 2007). All the UZ lithotypes experienced a post-Variscan exhumation and were subjected to variable degrees of serpentinization that in some instances erased the previous texture of peridotites.

The petrographic evidence of amphibole and minor dolomite requires carbon bearing hydrous metasomatic agents. The origin of the hydrous metasomatic fluids with a CO_2 component were at first interpreted by Rampone and Morten (2001) as residual fluids left after the crystallization of leucosomes of the host migmatite during the Variscan subduction. On the other hand, Scambelluri et al. (2006) emphasized that fluids interacted with the peridotites while the latter still resided in the mantle wedge (i.e. not within a crust-mantle mélange); moreover, the origin of metasomatic fluids were related to the reaction of hydrous anatectic melts with wedge peridotite at the slab-wedge boundary. This reaction produced an orthopyroxene-rich layer and LILE-rich residual fluids forming the garnet + amphibole peridotites. Later studies (Marocchi et al., 2007; Ionov et al., 2017) suggested that the migmatization of the host gneisses plausibly acted only during late stages of metasomatism, while the main metasomatic episodes were governed by slab-derived crustal fluids equilibrating with the lithospheric mantle prior to the Variscan subduction.

Dolomite, previously found in all UZ textural types, is the main C-repository (Sapienza et al., 2009; Förster et al., 2017; Gudelius et al., 2018). Trace elements analyses of dolomite from stage 2 and stage 3 peridotites indicate that dolomite represents the major repository also for Sr, Ba, Pb and subordinately LREE (Sapienza et al., 2009). Smaller amounts of magnesite are reported by Malaspina and Tumiati (2012) in a fine-grained porphyroclastic garnet peridotite and by Förster et al. (2017) in a coarse-grained protogranular peridotite. Only recently, evidences for carbonate dissolution-reprecipitation processes in these peridotites have been reported (Förster et al., 2017).

3. Analytical methods

Scanning electron microscopy (SEM), Electron probe microanalysis (EPMA)

Silicates, carbonates, oxides and sulfides were investigated with SEM and EPMA. Petrographic thick sections (ca. 100 μm of thickness) and peridotite chips with 5 mm of thickness were gold coated for SEM analyses. BSE images were acquired at the Dipartimento di Scienze Biologiche Geologiche e Ambientali, Università di Bologna, using a Scanning Electron Microscope (SEM) Philips 515B fitted with an EDAX DX4 microanalytical device. The operating conditions were: accelerating voltage of 15kV, beam current of 2nA and a spot size ~ 1μm. Major element compositions were determined with the JEOL 8100 SUPERPROBE electron microprobe at the Institute of Mineralogy and Petrography, University of Innsbruck, with the analytical conditions: 15 kV accelerating voltage, 10 nA beam current, using wavelength-dispersive spectroscopy (WDS). F-topaz (F), jadeite (Na_2O), orthoclase (K_2O), rutile (TiO_2), rhodonite (MnO), MgO, diopside (CaO), chromite (Cr_2O_3), almandine (FeO), corundum (Al_2O_3), atacamite (Cl), baryte (BaO), Ni-olivine (NiO), and quartz (SiO_2) were used as standards for silicates and oxides analyses, while calcite (CaO), diopside (MgO), strontianite (SrO), rhodonite (MnO) and almandine (FeO) standards were used for carbonates analyses. To avoid carbonate devolatilization during EPMA, the electron beam was defocused to an approximate size of 10x10 microns.

Micro-Raman spectroscopy

Micro-Raman spectroscopy was performed for the identification of the serpentine phases and calcite + brucite intergrowths at the Department of Mathematical, Physical and Computer Sciences, University of Parma. Polished thick sections and rock chips were investigated with a Horiba Jobin-Yvon LabRam apparatus, equipped with an Olympus microscope with 10x, 100x and ultra long working distance (ULWD) 50x objectives and motorized x-y stage. The 473.1 nm line of a doubled Nd:YAG diode pumped laser was used as excitation source with a spectral resolution of about 2 cm^{-1}. The 473.1 nm source was selected to work in the spectra range with the maximum sensitivity of the detector to enhance the OH stretching signal of the water molecules in the high wavenumber range (3000-4000 cm^{-1}). The spectra were collected using the ULWD 50X objective with repeated acquisition. The background subtraction of each spectrum was performed with the LabSpec® software.

In situ Laser Ablation MC-ICP-MS analyses

In situ Sr isotopes of carbonates occurring in three thick sections and four rock chips of 5 mm thickness, representing both fine- and coarse- grained peridotites, were measured at the Centro Interdipartimentale Grandi Strumenti (CIGS) of the University of Modena and Reggio Emilia (Italy) using a double focusing MC–ICP–MS with a forward Nier–Johnson geometry (Thermo Fisher Scientific, Neptune™), coupled to a 213 nm Nd:YAG laser ablation system (New Wave Research™). The analytical procedure is the same as of Giovanardi et al. (2018).

Laser ablation parameters consisted of a laser spot ranging from 55 µm to 100 µm (see Table 4), a fluence of ~10 J/cm^2, a laser frequency of ~10 Hz and a He flux of ~0.5 L/min. Signals were acquired in static mode with a block of 250 cycles (including laser warm-up, ~50–80 cycles of analysis and washout) and an integration time of 0.5 s. Collected *m/z* were 82Kr, 83Kr, 84Sr, 85Rb, 85.5, 86Sr, 86.5, 87Sr and 88Sr. Masses 85.5 and 86.5 were measured to check doubly charged Yb interferences. Kr was corrected measuring 60 s of gas blank with the laser off. After background subtraction, the remaining signal on mass 82 was used to check the formation of Ca dimers and argides; while mass 83 to check the presence of Er^{2+}. Rb was corrected by calculating the ^{87}Rb contribution to mass 87 by measuring the interference-free ^{85}Rb signal, correcting for instrumental mass fractionation, and using the natural $^{87}Rb/^{85}Rb$ ratio. Mass bias normalization was performed through exponential law and a $^{88}Sr/^{86}Sr$ ratio of 8.375209. The accuracy of the analyses was checked using an in-house reference material (modern marine shell) (see Table X in Supplementary Material), which yielded a $^{87}Sr/^{86}Sr$ ratio of 0.709174 ± 0.000064 (2σ; n = 19), in agreement with modern seawater (0.70917). Three analyses of a second in-house carbonate reference material yielded a $^{87}Sr/^{86}Sr$ ratio of 0.707562 ± 0.000018 (2σ), equal to the solution reference value (0.70756 ± 0.00003; 2σ) (Weber et al., 2019). Data reduction was performed using a customized excel spreadsheet.

4 Results

4.1 Sample description and petrography

Peridotite samples were collected from the Northeastern part of the UZ (Fig.s 1 and 3), from outcrops or boulders very close to the outcrops (Table 1 for sample description, location) (Fig.3). Each sample underwent weak up to very strong serpentinization that in some instances overprinted the previous textures. All the samples investigated contain carbonates such as dolomite and, locally, magnesite and calcite (see Table 1). From now on, the numbers 1 and 2 refer to first and second generation respectively of olivine, orthopyroxene, clinopyroxene and spinel.

Samples 18LP1 and MOL1-C are coarse-type spinel peridotites consisting mainly of large (1-4 mm) $olivine_1$, $orthopyroxene_1$ and $spinel_1$. Sample 18LP1 shows $orthopyroxene_1$ with undulose extinction and kink bands and they are usually surrounded by a chlorite rim with a diameter of about 150 μm. $Clinopyroxene_1$, exhibiting amphibole and spinel exsolutions, is associated with nearly-dark vermicular $spinels_1$. The studied chip rock contains a 300 μm wide veinlet crosscutting the matrix and filled with dolomite associated with colorless amphibole and chlorite; here, dolomite occurs as lobate-shaped grains (Fig. 5a). This veinlet is perpendicularly crosscut in several places by thin (ca. 50 µm wide) serpentine veins that locally contain dolomite streaks (ca. 25 µm wide) (Fig. 5b). Sample MOL1-C does not contain clinopyroxene$_1$ and mainly consists of strongly fractured olivines$_1$ and orthopyroxenes$_1$ showing kink bands. Vermicular dark spinel is often included in coarse green amphiboles. The sample shows a ca. 300 µm wide veinlet consisting of magnesite, serpentine, colorless amphibole and opaque minerals (Fig. 5c) cuts by a dolomite vein (ca. 200 µm long) (Fig. 5d). When the magnesite + serpentine + colorless amphibole vein encounters coarse crystals of orthopyroxene$_1$, serpentine minerals grow along orthopyroxene$_1$ cleavages promoting a black-colored needle-like serpentine microstructure (Fig.s 4a and 5c). Both coarse peridotites probably escaped full mineralogical equilibration under eclogite-facies conditions, as indicated by the absence of garnet.

Fine-grained peridotites are the most common textural rock type in the UZ. They show grain sizes smaller than 0.7 mm and exhibit porphyroblastic to equigranular textures. Sample VM10A is a fine-grained mylonitic garnet-amphibole-peridotite with a main foliation defined by the preferred orientation of matrix minerals. The main mineralogical association consists of fine-grained olivine$_2$, orthopyroxene$_2$, green amphibole, spinel$_2$ with accessory matrix dolomite (ca. 60 µm) (Fig. 5e) associated with apatite and green amphibole. Allanite locally occurs in the matrix. A porphyroclast (ca. 1cm) of highly fractured reddish zircon occurs in this rock; it contains a mm-sized dolomite inclusion associated with apatite. Rare small-sized pinkish-garnets occur.

Samples KL2.4-2b and KL2.4-3 are fine-grained garnet-amphibole peridotites and contain porphyroblasts of coarse pink garnet (ca. 1cm of size) surrounded by a kelyphitic corona made of orthopyroxene + amphibole + clinopyroxene ± spinel (Fig. 4b). These garnets are highly fractured and contain mm-sized spinel$_1$ inclusions. This spinel$_1$ locally hosts polycrystalline aggregates consisting of (i) apatite, ilmenite, pentlandite, calcite-brucite intergrowths and phlogopite; (ii) ilmenite, chlorite, apatite, pentlandite. The KL2.4-2b sample description is reported in detail by Förster et al. (2017), who also documented the occurrence of a dolomite inclusion (ca. 70 µm) in a primary spinel included in coarse-grained garnet. Matrix dolomite (ca. 40 µm) occurs commonly in association with green amphibole and apatite. In both samples, calcite occurs as thin veins in the matrix (Fig. 5g), included in chlorite and, in some instances, forming intergrowths with brucite. Two generations of serpentine minerals occur, with the first one represented by mesh structure in olivine$_2$ and bastite in orthopyroxene$_2$ and the second one forming thin veins crosscutting the matrix with the porphyroblastic garnet and keliphitic corona.

Sample KL1-A is a fine-grained garnet-amphibole peridotite with the same mineralogy of the previous samples but equigranular texture (ca. 300 µm) (Fig. 4c). Here, intergrowths of calcite + brucite associated with relict dolomite occur in the matrix (Fig. 5f). Widespread small-sized pinkish-garnets (200-300 µm) occur interstitially in the matrix, always exhibiting a kelyphitic corona of orthopyroxene + amphibole + clinopyroxene ± spinel. This peridotite sample shows mesh and bastite replacement textures of olivine and pyroxene respectively. This sample is also pervaded by thin veins of serpentine and chlorite crosscutting the matrix (Fig. 4c).

Sample MM1 is a fine-grained amphibole-chlorite peridotite. This sample comes from a well-studied outcrop which provided sample 300B studied by Morten and Obata (1990), Scambelluri et al. (2006) and Braga and Sapienza (2007). Particularity of the sample is the presence of a ca. 1 cm wide serpentine vein showing concentric zonation with a core filled by magnetite and pentlandite and minor dolomite and calcite, and a border zone including matrix minerals consisting of olivine$_2$, orthopyroxene$_2$, green amphibole and spinel$_2$ (see Figs. 5a-b-c-d and S1a-b-c-d in Supplementary Material). Matrix dolomite is estimated to occur with an abundance of 2%, with a grain-size range of about 50-100 μm and commonly associated with apatite (Figs. 5h and S1b in Supplementary Material).

4.2 Major element compositions and micro-Raman spectroscopy

Representative major element compositions of silicate minerals and apatites are listed in **Table 2** (for all the EPM analyses see Supplementary Material ST-I and ST-IX) while all the carbonates major element compositions are listed in **Table 3**. The major element compositions commonly do not exhibit variations between coarse-grained and fine-grained rocks and minerals of different generations. *Olivine* is unzoned with $Fo_{88-90}Teph_{0-2}$. *Orthopyroxene* is commonly $En_{90-92}Fs_{8-10}Wo_{0-1}$ with Al_2O_3 reaching values up to 2.80 wt.%. Two textural-types of *spinel* are recognized: a first generation of coarse $spinel_1$ included in porphyroblastic garnets exhibits Cr# ~ 0.43, where Cr# is Cr/(Cr+Al), while the second generation of matrix smaller $spinel_2$ has Cr# of about 0.35. *Clinopyroxene* is always diopside ($En_{46-49}Fs_{2-3}Wo_{47-50}$). Green *amphibole* in the matrix is commonly Mg-hornblende and minor pargasite (in samples KL2.4-2b and KL2.4-3). Pargasite is often rimmed by colorless *tremolitic amphibole* (Al_2O_3 ~ 0.25 wt.%). Considering the three amphibole-types, Na_2O and Al_2O_3 contents range from 0.1 to 1.6 wt.% and from 0.25 to 16.6 wt.%, respectively. When amphibole occurs in veinlets, its composition is always tremolitic (i.e. magnesite vein with tremolite and serpentine). Unzoned *garnet* is pyrope-rich ($Py_{51-70}Alm_{17-30}Sps_{1-4}Grs_{11-15}$) showing little to no compositional variations between porphyroclasts and small-sized garnets. *Apatite*, always in association with dolomite, exhibits a high Cl content of about 5 wt.%. Serpentine (*lizardite*) replacing olivine and pyroxenes exhibits a Fe content ranging from 1.53 to 9.02 wt.% FeO. In the fine-grained amphibole-chlorite peridotite sample MM1, a composite serpentine vein was characterized by micro-Raman spectroscopy showing lizardite and mixed lizardite/chrysotile compositions (Fig. S1 in Supplementary Material). Sheet silicates, represented by chlorite and phlogopite, show Fe contents of 2.22-2.55 and 3.45-5.03 wt.% FeO respectively. The Na_2O content of phlogopite reaches values of 0.13 wt.%.

Carbonate compositions are given in the $MgCO_3$-$CaCO_3$-$FeCO_3$ ternary diagram (Fig. 6). Unzoned *dolomite* does not exhibit any compositional variations between the different peridotites and microstructural domains. It can be classified as ferroan-dolomite, with X_{FeCO3} of about 0.02 in all the samples. Similarly, magnesite veinlet shows high Fe content, with X_{FeCO3} of about 0.05. *Calcite* (together with brucite) was identified using micro-Raman spectroscopy (see Fig S2 in Supplementary Material for the Raman spectrum), and it also occurs as thin veins cutting the matrix or as intergrowths with brucite in association with dolomite (Fig. 7). Calcite composition is close to the Ca-carbonate endmember (Fig. 6).

4.3 Sr isotope composition of Ulten Zone carbonates

In situ $^{87}Sr/^{86}Sr$ isotope ratio analyses are listed in **Table 4**. Carbonates were previously chosen and detected considering the grain size, the Sr concentration and the microstructural domain. Dolomite is the main C-repository, showing a grain size of mostly 30-70 μm. Calcite veins are too narrow (ca. 20-30 μm wide) to be measured by LA-MC-ICP-MS, while magnesite does not contain Sr (see Table IX in Supplementary Material). For this study we performed thirty-nine *in situ* analyses. Spot size analyses ranges between 55 and 100 μm, in relation to the carbonate size (see Table 4). The $^{87}Sr/^{86}Sr$ isotope ratios obtained for all the dolomites are reported in Figure 8 and range between 0.70360±0.00007 and 0.71184 ±0.00026 (n=36). The distribution of Sr isotopic compositions of all carbonates analyzed is shown in Figure 8.

In the coarse-type spinel peridotite *18LP1,* the dolomite vein associated with tremolite and chlorite exhibits highly variable Sr isotopic values ranging from 0.70360±0.00007 to 0.70830±0.00015 (n=12) (Figs. 8 and 9). Two lobate-shaped dolomite grains (spots 5, 8) shown in Figure 9 exhibit the lowest values of all UZ carbonates analyzed. In *MOL1-C* late vein dolomite cutting a magnesite vein (Fig. 5d) gives an average value of 0.71184 ±0.00026 (n=2), representing the highest radiogenic ratio obtained by the *in-situ* Sr measurements of all Ulten carbonates-bearing peridotites of this study.

In three fine-grained peridotites, both dolomite and (when possible) calcite were analyzed. In Figure 8 it can be observed that the Sr isotopic ratio of matrix dolomite is nearly-homogeneous within the same sample and, conversely, different values were obtained from the different fine-type peridotites. In the mylonitic garnet-amphibole peridotite *VM10A*, the $^{87}Sr/^{86}Sr$ ratio of matrix dolomite is 0.70529±0.00011 (n=4). In the same sample, a large dolomite inclusion (ca. 7 mm long) occurring in a zircon porphyroclast exhibits a $^{87}Sr/^{86}Sr$ ratio of 0.70597 ±0.00007, obtained by analyzing a line scan along the carbonate grain. In the fine-grained garnet-amphibole peridotite *KL1-A*, the dolomite $^{87}Sr/^{86}Sr$ ratio is 0.70671±0.00021 whereas calcite (associated to brucite) gives slightly higher radiogenic values of about 0.70719±0.00018 (n=3). It is worth noting that, given the small size of calcite and brucite and their textural interconnection, both of them were included in the spots analyses. However, brucite is not supposed to incorporate Sr^{2+} and we therefore consider our data as exclusive for calcite. Average value of matrix dolomite in fine-grained amphibole-chlorite peridotite *MM1* is 0.70487 ± 0.00010 (n=16).

5. Discussion

Petrographic data indicate that the UZ peridotites, during their complex metasomatic history, underwent carbonation and, locally, dolomite dissolution and calcite reprecipitation. To date, the crustal portion of the subducted continental slab has been considered as the source of the several metasomatic fluids that interacted with the UZ peridotites (Rampone and Morten, 2001; Scambelluri et al., 2006; Sapienza et al., 2009). The presence of hydrous phases (dissakisite-Ce, amphibole and minor phlogopite) enriched in LILE, Th, U, and LREE compared to other incompatible trace elements, as well as the occurrence of large zircon grains (Forster et al., 2017; this study), strongly support this interpretation. On the basis of textures, bulk rock and mineral major and trace element compositions, Ionov et al. (2017) suggested that most of the "crustal" overprint of the UZ occurred into the mantle wedge well below the crust (ca. 850°C at 60-90 km depths), in a supra-subduction setting similar to the mantle wedge sampled by harzburgite xenoliths from the western Pacific. Given the uncertainty of 'crustal' vs 'mantle' origin of metasomatizing fluids, the Sr concentration and isotopic signature of carbonates of the UZ peridotites may help to shed light on these contrasting views.

We will focus on C-related processes by simply dividing the metasomatic evolution into two main stages: (1) the *HP* carbonation of mantle wedge peridotites at peak (eclogite-facies) conditions and during their early exhumation up to mid-crust depth and (2) the carbon re-mobilization via fluid-rock interaction during the final exhumation of the crust-mantle mélange, which formed after the incorporation of mantle slivers into the subducted continental crust. The tectonic insertion of the peridotites into the host gneiss is believed to have occurred after peak pressure conditions (Scambelluri et al. 2006). We discuss these two processes separately, referring to them as Stage1 and Stage 2.

5.1 Stage 1: HP carbonation.

Included and interstitial dolomite

The onset of the metasomatic history of the UZ peridotites started with percolation of melts into the spinel-facies mantle wedge, causing the formation of pyroxenite layers (Nimis and Morten, 2000). At this stage there is no petrographic evidence of carbonation. Conversely, the occurrence of lobate-shaped dolomite inclusion in a porphyroclastic zircon and matrix dolomites in the fine-grained, garnet-bearing peridotites suggests that carbonation occurred when the Ulten peridotites reached peak eclogite-facies conditions (Fig.10). If zircon and dolomite formation are coeval as the petrographic observation suggests, a time constraint for this early episode of carbonation can be provided by the 333 Ma U-Pb age of zircon from metasomatic reaction bands at the Mt. Hochwart gneiss-peridotite contact (Tumiati et al., 2007), the same locality of sample VM10A of this study.

Furthermore, in another fine-grained garnet-bearing peridotite we have a unique microstructural evidence of a dolomite inclusion in Cr-spinel, which is included in a porphyroclastic garnet. Major elements composition obtained with EPMA shows that this inclusion has the same composition as the matrix dolomite and dolomite veins. The origin of this inclusion is yet unknown (i.e. mantle provenance or subducted continental crustal derivation), but the occurrence of fractures in the host garnet may suggest that dolomite precipitation could have been induced during C-rich fluids percolation after spinel and garnet crystallization (in contrast to the interpretation of an early melt-related process in the high-*T* spinel stage given by Förster et al., 2017). At peak conditions, fluids prompted the precipitation of interstitial dolomite.

During continental collision, the crustal portion of the descending slab consists of the sedimentary cover and its underlying crystalline basement. The subducted lithologies may release fluids into the overhanging mantle wedge and their source can be investigated, at least in part, by considering fluid mobile elements (FME) such as Sr and the $^{87}Sr/^{86}Sr$ isotopic ratio. Different sources of the metasomatic liquids were considered for the *HP*-dolomite (both included and interstitial), as reported in Figure 11: (i) associated stromatic gneisses and orthogneisses; (ii) Devonian sedimentary cover; (iii) lithospheric mantle; (iv) trondhjemitic dykes and pockets.

(i) Based on literature, we expected similar Sr isotopic ratio for the carbonates and the associated crustal rocks. However, the high $^{87}Sr/^{86}Sr$ ratio of stromatic gneisses (i.e. migmatitic paragneisses that suffered 20-30% degree of partial melting according to Braga and Massonne, 2012) and orthogneisses from the subducted crust and now part of the mélange, argues against their role as the sources for C-bearing fluids.

(ii) It is difficult to assess the role of a sedimentary cover overlying the crystalline basement because of the lack of field evidence of Paleozoic sedimentary successions associated with the UZ crust-peridotite association. Subducted marine carbonates along the oceanic crust subduction prior to the subduction of the continental crust may also play a role in the formation of carbonates in the mantle wedge. However, Sr isotope values reported by van Geldern et al. (2006) for well-preserved Devonian brachiopod shells (Mn < 100 ppm; Fe < 400 ppm and Sr > 500 ppm) range from 0.70782 to 0.70804 (during the Emsian-Eifelian boundary and early Famennian respectively), unlikely representing the required sources for the interstitial dolomite in the matrix.

(iii) The relatively unradiogenic values of matrix carbonates have Sr isotopic values close to those of the coarse-grained spinel-garnet peridotites of Tumiati et al. (2003), as shown in Fig. 11. Several studies (i.e. Tumiati et al. 2003 and Scambelluri et al. 2006) highlighted that the UZ peridotites were enriched in incompatible elements by reacting with fluids released from a subducting continental lithosphere undergoing partial melting. In particular, the enrichment of the UZ peridotite took place in the mantle wedge above the subduction zone (Scambelluri et al. 2006) by fluids variably equilibrated with mantle rocks (Ionov et al. 2017). In this scenario, the fluids responsible for the formation of matrix dolomite might have variably reacted with a depleted lithospheric mantle and evolved towards slightly lower Sr isotopic compositions before crystallizing matrix dolomite.

(iv) The radiogenic Sr signature of few trondhjemitic dykes and pockets described by Del Moro et al. (1999) are close to those reported for the matrix dolomite of the fine-grained mylonitic garnet-amphibole peridotite VM10A from Mt. Hochwart. Based on petrology and whole-rock Sr-Nd isotope geochemistry, Del Moro et al. (1999) interpreted the UZ trondhjemite as melts produced by fluid-assisted anatexis of a metasedimentary lower crust characterized by low Rb/Sr and Sr isotope ratios. Once formed, the trondhjemite melts intruded the UZ migmatitic crust.

Localized carbonation: carbonates veinlets.

The tectonic insertion of mantle material into the crustal portion of the continental slab occurred after the attainment of maximum pressure conditions, i.e. at the beginning of the exhumation (Scambelluri et al., 2006). During this early phase of upwelling of the crust-mantle mélange, dolomite veins associated with tremolite and chlorite and magnesite + lizardite-crysothile + tremolite vein within the two coarse-type spinel peridotites are indicative that carbonation occurs as local injection of C-rich fluids (Fig. 10) under different retrograde *P*-*T* conditions. The mineral assemblage of the dolomite + tremolite + chlorite vein supports the evidence of a retrograde process prior to serpentinization (650°C≤ T≤700°C at *P* of ca. 1 GPa) and, in addition, provides a minimum *P*-*T* estimate for the formation of the crust-mantle mélange.

The Sr isotopic heterogeneity (0.7035-0.7085; Figs. 8 and 9) measured in different dolomite grains from the dolomite + tremolite + chlorite vein encompasses the ^{87}Sr/^{86}Sr values measured from matrix and included dolomite. Most of the inter-grain variability can be explained by the interaction of the matrix and the included dolomite, which show low-Sr isotopic values, with progressively more radiogenic fluid, as it would be expected in mantle rocks closely associated with crustal lithologies. Similarly, late-stage carbonate veins in kimberlites from Beinfontein show a large variability of the Sr-isotope composition, reaching values of 0.70957$\pm$116 (2σ). These results were interpreted as a consequence of primary carbonates interaction with crustal fluids (Castillo-Oliver et al., 2018), as we speculate for the UZ dolomite veins. It is not easy to explain the occurrence of low ^{87}Sr/^{86}Sr ratios (0.7036-0.7039; Figs. 8 and 9) of two dolomite grains in this vein. As shown in Fig. 11, these values approach the MORB signature, thus requiring a distinct metasomatic agent with a Sr signature typical of a mantle reservoir depleted in radiogenic Sr. This metasomatic agent depleted in radiogenic Sr precipitated primary carbonates that did not interact with late-stage metasomatic crustal fluids.

The occurrence of a magnesite vein associated with lizardite-chrysotile and tremolite suggests influx of a local carbonaceous fluid at T < 600°C during the retrograde path. This vein is cut by a dolomite vein with the highest $^{87}Sr/^{86}Sr$ ratio (0.7118-0.7119; Figs. 5d and 8), which formed after the previously discussed vein dolomite. The highly radiogenic values of this vein suggest that this episode of injection of C-rich fluids occurred when the orogenic mélange, characterized by mingled crustal and mantle components, was already well developed and that infiltrating C-rich crustal fluids introduced significant amounts of radiogenic Sr (Fig. 11). According to the geodynamic scenario of Ranalli et al. (2005), this mélange was brought to mid-crustal depths between 330 and 300 Ma reaching 0.7 GPa at 500°C.

5.2 Stage 2. Carbon re-mobilization via fluid-rock interaction

Following the geodynamic model proposed by Ranalli et al. (2005), after the late Carboniferous fast exhumation, the crust-mantle mélange underwent slow exhumation and cooling during Permian-Triassic times (300-205 Ma). During this slow exhumation, Stage2 carbonation is related to the action of serpentinizing fluids, which in some instances erased the previous mantle texture. Here, C re-mobilization via fluid-rock interaction prevails (blue arrow, Fig. 10) as evidenced by the occurrence of (i) calcite + brucite intergrowths surrounded by serpentine (Figs. 5f and 7) and (ii) thin calcite veins.

The calcite + brucite intergrowths are the result of dolomite breakdown during interaction with aqueous fluids (Figs. 5f and 7) (Förster et al., 2017) and were found only in highly serpentinized fine-grained garnet-bearing peridotites. Moreover, micro-Raman investigations allowed the identification of lizardite as the serpentine phase surrounding these intergrowths. If serpentinizing fluids were the cause of dolomite dissolution, we therefore argue that the precipitation of calcite + brucite probably occurred at P of about 0.5 GPa and $T < 300°C$. At this stage the Ulten basement was likely subjected to isostatic adjustment after the conclusion of the Variscan collision (Ranalli et al., 2005).

The formation of thin calcite veins occurring in the matrix and in some instances crosscutting spinel, chlorite and phlogopite, was interpreted by Förster et al. (2017) as a consequence of the influx of serpentinizing fluids that triggered dissolution of the former dolomite and crystallization of calcite + brucite intergrowths with concomitant liberation of CO_2, following the reaction $CaMg(CO_3)_2 + H_2O \rightarrow CaCO_3 + Mg(OH)_3 + CO_2$. The release of CO_2 may prompt *in-situ* formation of carbonates (i.e. thin calcite veins) after C saturation was achieved.

During fluid-rock interaction, Sr preferentially partitions into the fluid phase (Banner et al., 1995) and the aqueous serpentinizing fluids, characterized by $^{87}Sr/^{86}Sr \approx 0.7070\text{-}0.7075$, dissolved dolomite that provided the local source of Sr. Eventually, the fluid enriched in C and Sr (from dolomite) precipitated relatively Sr-rich calcite. The higher elemental Sr abundance with respect to dolomite is due to the less incompatible behavior of Sr in calcite (Banner et al., 1995).

6. Conclusion and future directions

The combination of textural observation of carbonates with *in situ* Sr isotope analyses reveals a more complex metasomatic evolution for the UZ peridotite than previously thought. In particular, two main conclusions can be drawn: (1) at peak (eclogite facies) conditions, there is not a simple carbon transfer between the crustal portion of a subducted continental and the overhanging wedge, but additional C sources have to be considered and (2) at low-pressure conditions, during the final exhumation stages of an already well developed crust-mantle mélange, the main carbonation process implies dolomite breakdown and calcite reprecipitation by H_2O-rich fluids.

The relatively unradiogenic Sr isotope ratio recorded by includsion- and matrix dolomite, with some grains of a dolomite vein, does not support a simple derivation from fluids derived from the migmatite host gneisses (Fig. 11). The first stage of carbonation thus requires *HP* metasomatic fluids (i.e. at ~ 2.5 GPa and 850°C) likely unrelated to the associated crust (stromatic gneisses and orthogneisses), as already recognized by Marocchi et al. (2009; 2007). We suggest that these *HP* fluids may have variably equilibrated with a depleted lithospheric mantle before the crystallization of matrix dolomite. Residual COH fluids originated from the crystallization of trondhjemite liquids intrusion derived from deeper portions of the Ulten crust or fluids released from Paleozoic carbonate succession and involved into the Variscan orogenesis can be considered as alternative sources for the metasomatic agents infiltrating at peak conditions and before the onset of serpentinization.

During the first stages of exhumation, C-bearing fluids were channeled into veins, giving rise to the veinlet filled with dolomite associated with tremolite and chlorite, followed at lower *P*-*T* conditions by the formation of the magnesite + lizardite-crysothile + tremolite veins. The fluids released by the crystallization of leucosomes of the host migmatites, showing variable CO_2/H_2O ratios as inferred by Rampone and Morten (2001), seem to be important metasomatic agents only at the end of the exhumation of the crust-mantle mélange, at temperatures consistent with lizardite stability, providing the highest Sr isotope values for the dolomite veins. The infiltration of serpentinizing fluids represents the last metasomatic episode of peridotites, leading to C-remobilization by dolomite dissolution and calcite precipitation with concomitant liberation of CO_2.

Evidences of both H*P* carbonation and carbonates dissolution-reprecipitation make these rocks an effective carbon locker and a “pit-stop” for C-remobilization through a mantle wedge. Consequently, the results of this study have implications for the global comprehension of the so called “Deep Carbon Cycle”. While in situ Sr isotope data have demonstrated useful to give us additional constrains on an overall complex multiphase metasomatic evolution, their main limitation is the restriction to relatively large grains ($\geq 50 \mu m$) and the less precision compared to dilution techniques. However, our approach ensures the textural control that is mandatory when multiple generations of metasomatic minerals occur in the same sample. The errors obtained for the Ulten carbonates, moreover, are far lower than the variability observed, allowing to clearly distinguish the different isotope patterns. Future higher resolution in-situ C and O isotope analyses of carbonates will allow to better constrain the sources of these C-bearing metasomatizing fluids.

Acknowledgements

G. Gasparotto (University of Bologna), M. Tribus (University of Innsbruck) and Antonio Langone are thanked for assistance during SEM, EPMA and LA-ICP-MS analyses. Constructive reviews by Guilleume Delpech and Andrea Giuliani greatly improved this work. This research was supported by RFO and ALMAIDEA grants (University of Bologna).

References

Banner, J.L., 1995. Application of the trace element and isotope geochemistry of strontium to studies of carbonate diagenesis. Sedimentology 42, 805–824.

Bebout, G.E., Penniston-Dorland, S.C., 2016. Fluid and mass transfer at subduction interfaces. The field metamorphic record. Lithos 240, 228–258.

Braga, R., Sapienza, G.T., 2007. The retrograde evolution of a dolomite-bearing hydrous peridotite from the Ulten Zone (Italian Alps). GeoActa 6, 37–45.

Braga, R., Massonne, H.-J., 2012. H_2O content of deep-seated orogenic continental crust: the Ulten Zone, Italian Alps, International Geology Review 54, 633–641.

Brueckner, H.K., Medaris, L.G., 2000. A general model for the intrusion and evolution of ‘mantle’garnet peridotites in high-pressure and ultra-high-pressure metamorphic terranes. Journal of Metamorphic Geology 18, 123–133.

Castillo-Oliver, M., Giuliani, A., Griffin, W., L., O’Reilly, S., Y., 2018. Characterisation of primary and secondary carbonates in hypabyssal kimberlites: an integrated compositional and Sr-isotopic approach. Mineralogy and Petrology, 112, S555–S567.

Del Moro, A., Martin, S., Prosser, G., 1999. Migmatites of the Ulten Zone (NE Italy), a record of melt transfer in deep crust. Journal of Petrology 40, 1803–1826.

Dickin, A.P., 2018. Radiogenic isotope geology. 3rd edition, Cambridge University Press, 482.

Evans, B.W., Johannes, W., Oterdoom, H., Trommsdorff, V. 1976. Stability of chrysotile and antigorite in the serpentinite multisystem. Schweizerische Mineralogische und Petrographische Mitteilungen, 56, 79–93.

Förster, B., Braga, R., Aulbach, S., Pò, D.L., Bargossi, G.M.G.M., Mair, V., 2017. A petrographic study of carbonate phases in the Ulten Zone ultramafic rocks: insights into carbonation in the mantle wedge and exhumation-related decarbonation. Ofioliti 42, 105–127.

Fumagalli, P., Poli, S., 2005. Experimentally determined phase relations in hydrous peridotites to 6.5 GPa and their consequences on the dynamics of subduction zones. Journal of Petrology, 46, 555–578.

Gasparrini, M., Bechstädt, T., Boni, M., 2006. Massive hydrothermal dolomites in the southwestern Cantabrian Zone (Spain) and their relation to the Late Variscan evolution. Marine and Petroleum Geology 23, 543-568.

Giovanardi, T., Mazzucchelli, M., Lugli, F., Girardi, V.A., Correia, C.T., Tassinari, C.C., Cipriani, A., 2018. Isotopic constraints on contamination processes in the Tonian Goiás Stratiform Complex. Lithos 310, 136–152.

Godard, G., Martin, S., Prosser, G., Kienast, J.R., Morten, L., 1996. Variscan migmatites, eclogites and garnet-peridotites of the Ulten zone, Eastern Austroalpine system. Tectonophysics 259, 313–341.

Gudelius, D., Aulbach S., Braga, R., Höfer, H., Woodland, A.B., Gerdes A., 2018. Element transfer and redox conditions in continental subduction zones: new insights from peridotites of the Ulten Zone, North Italy. Journal of Petrology 60, 231–268.

Hermann, J., Zheng, Y.-F., Rubatto, D., 2013. Deep fluids in subducted continental crust. Elements 9, 281–287.

Ionov, D.A., Bigot, F., Braga, R., 2017. The Provenance of the Lithospheric Mantle in Continental Collision Zones: Petrology and Geochemistry of Peridotites in the Ulten–Nonsberg Zone (Eastern Alps). Journal of Petrology 58, 1451–1472.

Johannes, W., Puhan, D., 1971. The calcite-aragonite transition, reinvestigated. Contributions to Mineralogy and Petrology 31, 28–38.

Malaspina, N., Tumiati, S., 2012. The role of COH and oxygen fugacity in subduction-zone garnet peridotites. European Journal of Mineralogy 24, 607–618.

Manning, C.E., 2014. A piece of the deep carbon puzzle. Nature Geoscience 7, 333.

Marocchi, M., Hermann, J., Morten, L., 2007. Evidence for multi-stage metasomatism of chlorite-amphibole peridotites (Ulten Zone, Italy): constraints from trace element compositions of hydrous phases. Lithos 99, 85–104.

Marocchi, M., Mair, V., Tropper, P., Bargossi, G.M., 2009. Metasomatic reaction bands at the Mt. Hochwart gneiss-peridotite contact (Ulten Zone, Italy): insights into fluid-rock interaction in subduction zones. Mineralogy and Petrology 95, 251–272.

Martin, S., Godard, G., Prosser, G., Schiavo, A., Bernoulli, D., Ranalli, G., 1998. Evolution of the deep crust at the junction Austroalpine/Southalpine: the Tonale Nappe. Memorie di Scienze Geologiche 50, 3–50.

Morten, L., Obata, M., 1990. Rare earth abundances in the eastern Alpine peridotites, Nonsberg area, Northern Italy. European Journal of Mineralogy 643–654.

Müller, W., Prosser, G., Mancktelow, N.S., Villa, I.M., Kelley, S.P., Viola, G., Oberli, F., 2001. Geochronological constraints on the evolution of the Periadriatic Fault System (Alps). International Journal of Earth Sciences 90, 623–653.

Nimis, P., Morten, L., 2000. P–T evolution of ‘crustal’ garnet peridotites and included pyroxenites from Nonsberg area (upper Austroalpine), NE Italy: from the wedge to the slab. Journal of Geodynamics 30, 93–115.

Obata, M., Morten, L., 1987. Transformation of spinel lherzolite to garnet lherzolite in ultramafic lenses of the Austridic crystalline complex, northern Italy. Journal of Petrology 28, 599–623.

Petrini, R., and Morten, L., 1993. Nd-isotopic evidence of enriched lithospheric domains: an example from the Nonsberg area, Eastern Alps. Terra Nova 5, 19–20.

Rampone, E., Morten, L., 2001. Records of crustal metasomatism in the garnet peridotites of the Ulten Zone (Upper Austroalpine, Eastern Alps). Journal of Petrology 42, 207–219.

Ranalli, G., Martin, S., Mahatsente, R., 2005. Continental subduction and exhumation: an example from the Ulten Unit, Tonale Nappe, Eastern Austroalpine. Geological Society, London, Special Publications 243, 159–174.

Salters, V.J.M. and Stracke, A., 2004. Composition on the depleted mantle. Geochemistry Geophysics Geosystems 5, 1–27.

Sapienza, G.T., Scambelluri, M., Braga, R., 2009. Dolomite-bearing orogenic garnet peridotites witness fluid-mediated carbon recycling in a mantle wedge (Ulten Zone, Eastern Alps, Italy). Contributions to Mineralogy and Petrology 158, 401–420.

Scambelluri, M., Hermann, J., Morten, L., Rampone, E., 2006. Melt-versus fluid-induced metasomatism in spinel to garnet wedge peridotites (Ulten Zone, Eastern Italian Alps): clues from trace element and Li abundances. Contributions to Mineralogy and Petrology 151, 372–394.

Schramke, J.A., Kerrick D.M., Blencoe J.G., 1982. Experimental determination of the brucite = periclase + water equilibrium with a new volumetric technique. American Mineralogist 67, 269–276.

Tumiati, S., Thöni, M., Nimis, P., Martin, S., Mair, V., 2003. Mantle–crust interactions during Variscan subduction in the Eastern Alps (Nonsberg–Ulten zone): geochronology and new petrological constraints. Earth and Planetary Science Letters 210, 509–526.

Tumiati, S., Godard, G., Martin, S., Klötzli, U., Monticelli, D., 2007. Fluid-controlled crustal metasomatism within a high-pressure subducted mélange (Mt. Hochwart, Eastern Italian Alps). Lithos 94, 148–167.

Tumiati, S., Fumagalli, P., Tiraboschi, C., Poli, S., 2013. An experimental study on COH-bearing peridotite up to 3.2 GPA and implications for crust-mantle recycling. Journal of Petrology 54, 453–479.

Van Achterbergh, E., Ryan, C.,G., Jackson, S.E., Griffin, W.,L., Sylvester, P., 2001. Laser-Ablation-ICPMS in the Earth Sciences- Principles and Applications. Mineralogical Association of Canada. 239–243.

van Geldern, R., Joachimski M.M., Day, J., Jansen, U., Alvarez, F., Yolkin E.A., Ma, X.,-P., 2006. Carbon, oxygen and strontium isotope records of Devonian brachiopod shell calcite. Paleogeography, Palaeoclimatology, Palaeoecology 240, 47–67.

Weber, M., Lugli, F., Hattendorf, B., Scholz, D., Mertz-Kraus, R., Guinoiseau, D., Jochum, K.P. (2019) NanoSr-A – new carbonate microanalytical reference material for *In situ* Strontium isotope analysis. Geostandards and Geoanalytical Research doi.org/10.1111/ggr.12296.

Whitney, D.L., Evans, B.W., 2010. Abbreviations for names of rock-forming minerals. American Mineralogist 95, 185–187.

Zanetti, A., Mazzucchelli, M., Rivalenti, G., Vannucci, R., 1999. The Finero Phlogopite-Peridotite Massif: An example of subduction-related metasomatism. Contributions to Mineralogy and Petrology 134, 107–122.

Zheng, Y.-F., 2012. Metamorphic chemical geodynamics in continental subduction zones. Chemical Geology 328, 5–48.

Zheng, Y.-F., 2009. Fluid regime in continental subduction zones: petrological insights from ultrahigh-pressure metamorphic rocks. Journal of the Geological Society 166, 763–782.

Figure captions – Preference color: online only

Fig.1: Geological sketch map of the study area: localization of the Ulten Zone in the Northeastern Alps and simplified geological map of the Ulten Zone from the 1:10.000 sheets Appiano and Rabbi of the Italian Geological Map with samples localization.

Fig. 2: *P-T* trajectory of the Ulten Zone peridotites. Infiltration of hot deep melt (red oval) into wedge peridotites in the spinel stage (Stage1); downward flow of wedge peridotites close to the slab-wedge interface due to corner flow (Stage2); exhumation after incorporation of peridotites in a crust-mantle mélange (Stage 3). Redrawn after Nimis and Morten (2000) and Scambelluri et al. (2006).

Fig.3: The Ulten Zone peridotites in the field. (a) Overview of the geological setting close to Malga Masa Murada with indication of the peridotites outcrop showed in detail in (b); (c)-(d) Serpentinized fine-grained peridotites; (e) Highly altered coarse-grained peridotite with coarse orthopyroxenes.

Fig.4: Overview of (a) Coarse-grained spinel peridotite MOL1-C with its characteristic serpentine + magnesite + tremolite vein. See text for detailed description. (b) Fine-grained porphyroblastic-garnet-bearing peridotite KL2.4-3. Pinkish-garnet is surrounded by keliphytic corona and includes larges spinels with polycrystalline aggregates. In this peridotite serpentine is common, in association with magnetite. (c) Fine-grained garnet-bearing peridotite KL1-A. Mineral abbreviations after Whitney and Evans (2010).

Fig.5: BSE images of carbonates from the Ulten Zone peridotite. (a) 18LP1. Lobate-shaped dolomite grains constituting a veinlet with tremolite and chlorite; (b)18LP1. Dolomite streaks into serpentine vein; (c) MOL1-C. Serpentine vein with magnesite and tremolitic amphibole. Infiltration of the vein into orthopyroxene formed spectacular needle-shaped microstructure with opaque minerals; (d) MOL1-C. Dolomite vein cutting the magnesite veinlet; (e) VM10A. Interstitial dolomite with its perfect cleavage; (f) KL1-A. Matrix dolomite associated with apatite. Note the incipient formation of calcite-brucite intergrowths into dolomite; (g) KL2.4-3. Large spinel cut by a

thin calcite vein; (h) MM1. Matrix dolomite (with little magnesite inclusions) associated with apatite and serpentine. Mineral abbreviations after Whitney and Evans (2010).

Fig.6: Carbonates composition plotted in the $MgCO_3$-$CaCO_3$-$FeCO_3$ ternary diagram.

Fig.7: BSE image of calcite-brucite intergrowths occurring in fine-grained garnet-amphibole peridotite KL1-A. The stars point out the spots for micro-Raman analyses whose spectra is reported in Fig.9. The yellow arrows indicate the serpentine surrounding calcite-brucite intergrowths. Mineral abbreviations after Whitney and Evans (2010).

Fig.8: Sr isotope ratios for dolomites and calcites occurring in different microstructural positions measured by LA-MC-ICP-MS. The error bars represent ± 2 standard errors. Whole rock $^{87}Sr/^{86}Sr$ for fine-grained garnet-amphibole peridotite A4323 and coarse-grained spinel-garnet peridotite A4454 from the work of Tumiati et al. (2003) are reported for comparison.

Fig.9: Partial sketch of a dolomite vein associated with tremolite and chlorite in sample 18LP1 with SEM-BSE images associated. Analyzed spots with Sr isotope ratio are reported.

Fig.10: *P*-*T* diagram with stages of carbonates formation during the metasomatic evolution of the Ulten peridotites. See text for discussion. Reference curves: Dolomite-in, magnesite-in, dolomite-out, garnet-in curve from Tumiati et al., (2013); tremolite (Tr) + magnesite (Mgs) = enstatite (En) + dolomite (Dol) from Malaspina and Tumiati (2012) for $X_{CO2} = 0.5$; brucite (Brc) = periclase (Per) + water (H_2O) from Schramke et al., (1982). Antigorite-out curve and chlorite-out curve from Fumagalli and Poli (2005). Antigorite = chrysotile (Ctl) / Lizardite (Liz) from Evans (1976); aragonite = calcite from Johannes and Puhan (1971). The H*P*-garnet stage and chlorite-amphibole

stage correspond to the thermobarometric data obtained by Nimis and Morten (2000) and Sapienza et al. (2009). Mineral abbreviations after Whitney and Evans (2010).

Fig.11: Strontium isotopic compositions of carbonates from the Ulten Zone peridotites in comparison with the potential sources of C-bearing fluids. MORB values taken from Salters and Stracke (2004); the Sr-isotope values of stromatic gneisses and peridotites from Tumiati et al. (2003) and the stromatic gneisses, orthogneisses and trondhjemitic intrusions from Del Moro et al. (1999) are recalculated for t=330Ma, corresponding to the inferred age of the last isotopic homogenization event. The Sr-isotope values for the brachiopod shell calcites from van Geldern et al. (2006) correspond to Early to Late Devonian (Emsian-Eifelian boundary and early Famennian).

Figure1

Fig.1

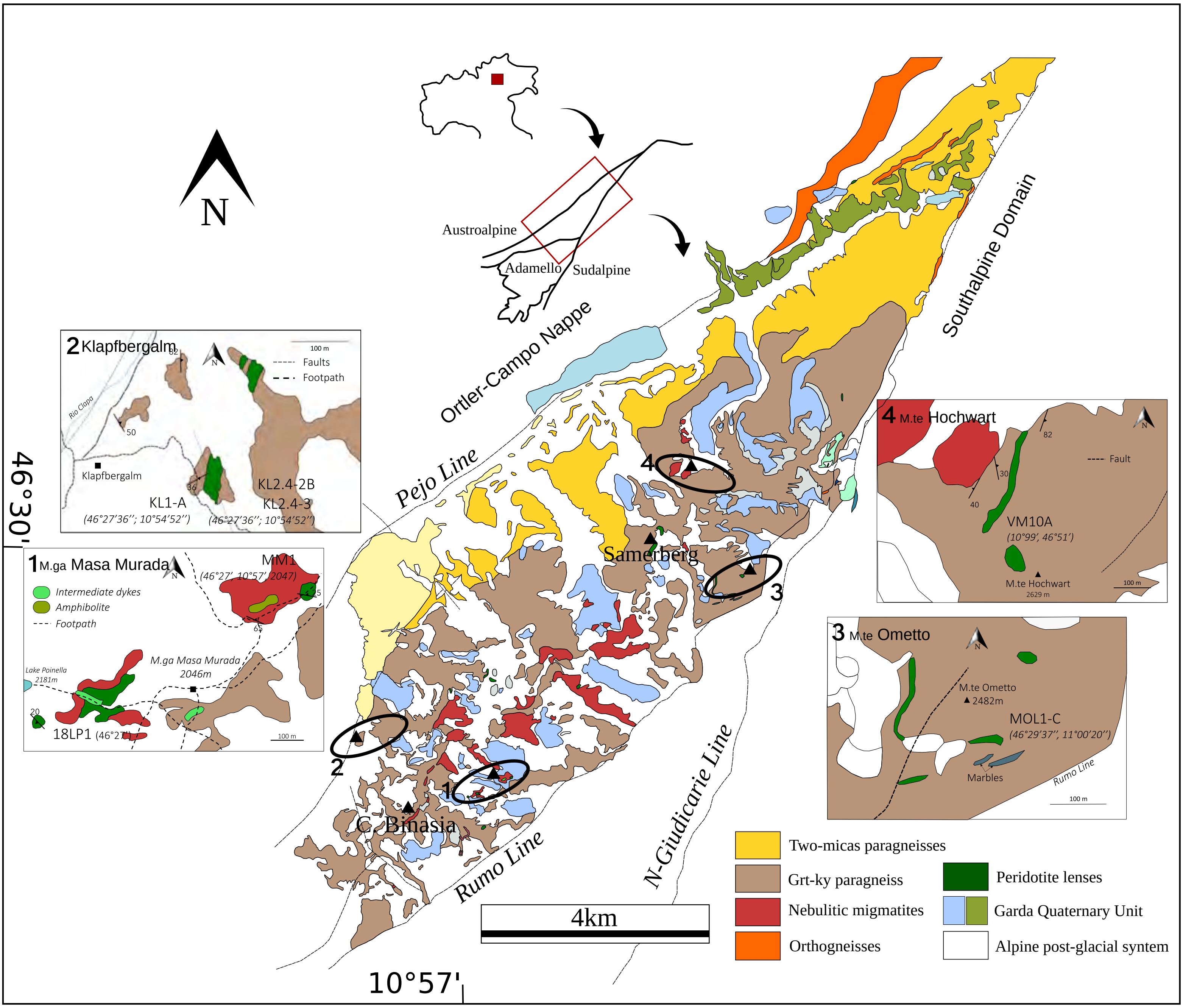

Figure2

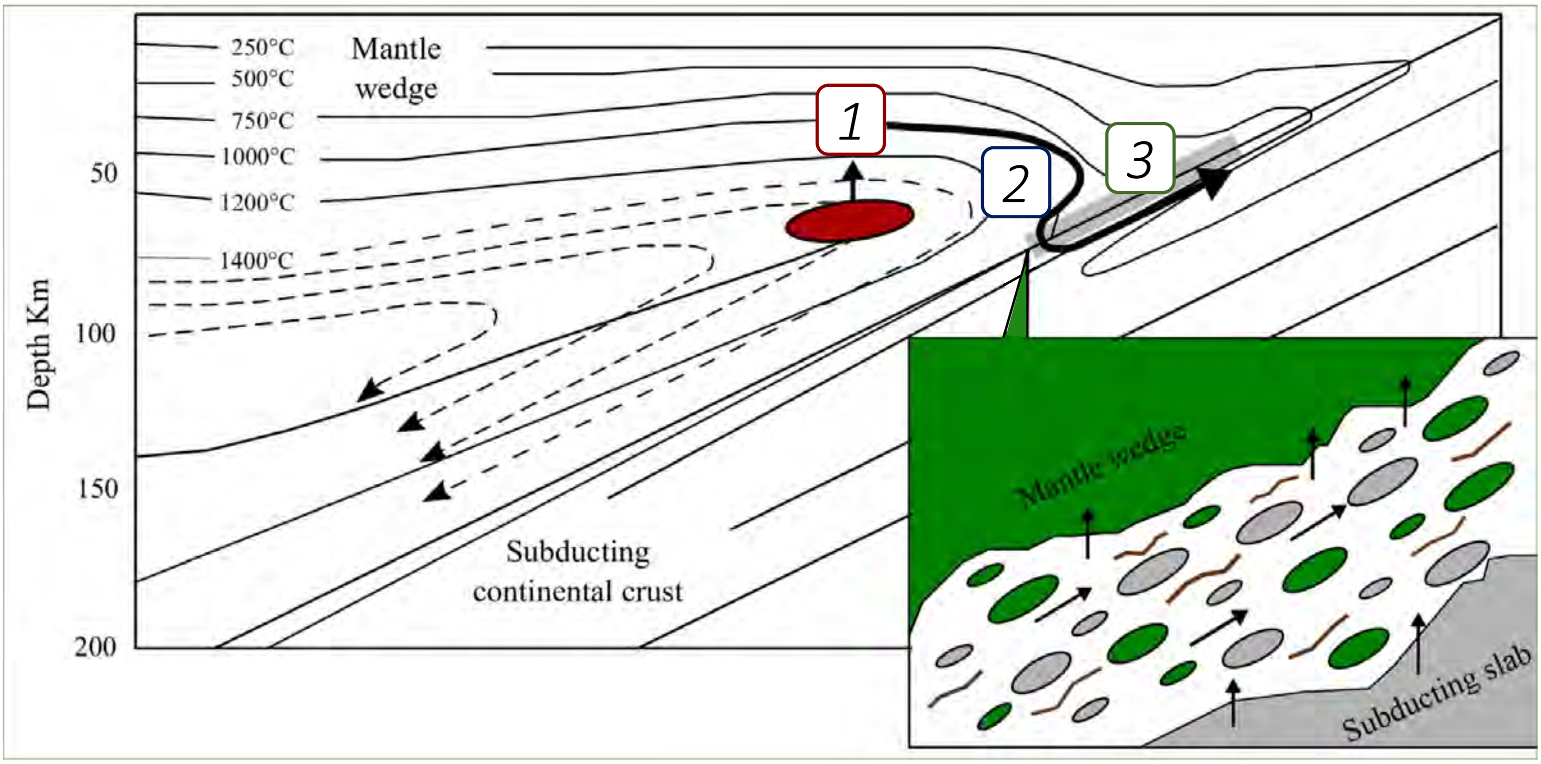
250°C
500°C
750°C
1000°C
1200°C
1400°C
Mantle wedge
1
2
3
Depth Km
50
100
150
200
Subducting continental crust
Mantle wedge
Subducting slab

Figure3

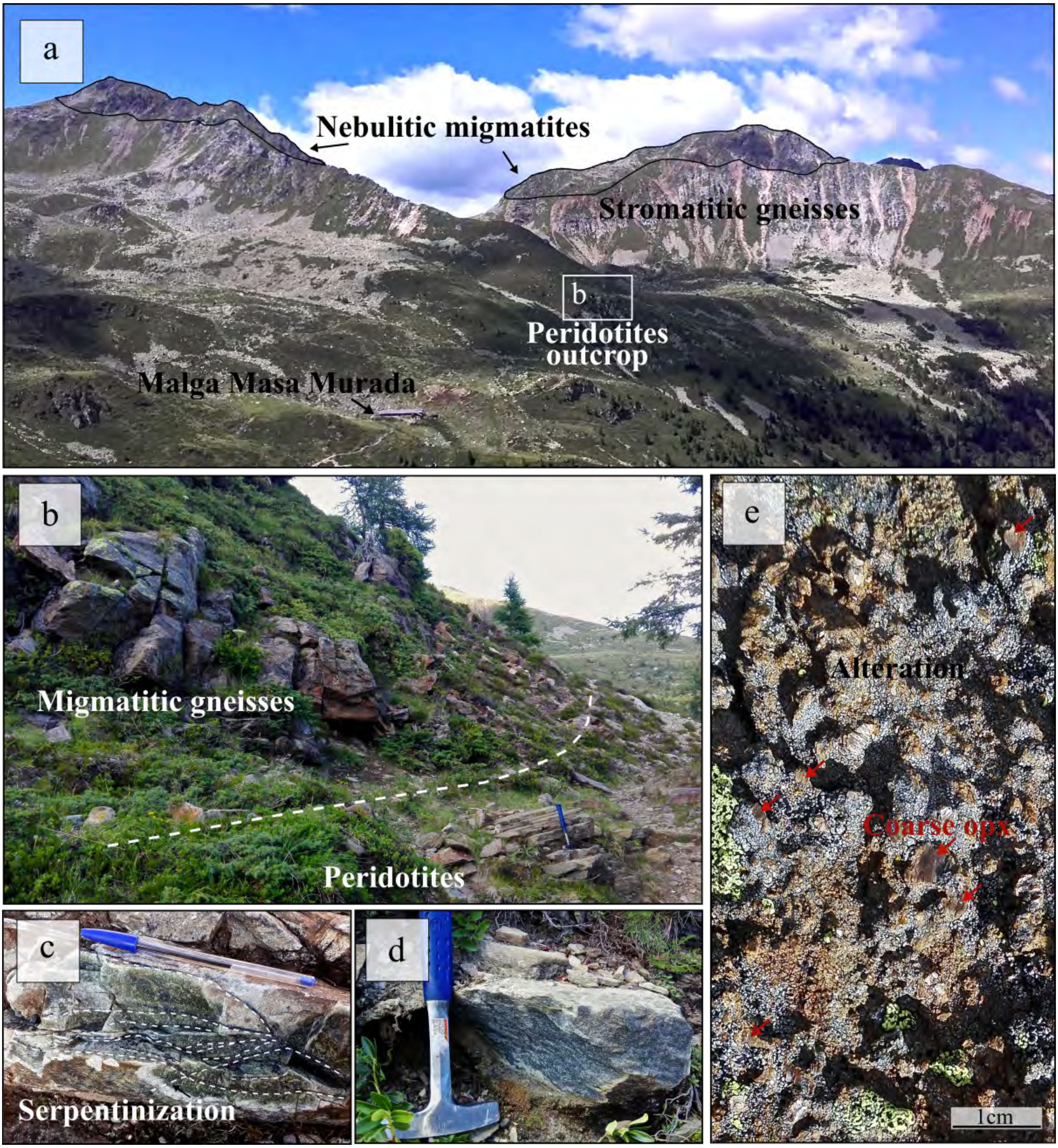
a
Nebulitic migmatites
Stromatitic gneisses
b
Peridotites
outcrop
Malga Masa Murada
b
Migmatitic gneisses
Peridotites
c
Serpentinization
d
e
Alteration
Coarse opx
1cm

Figure4

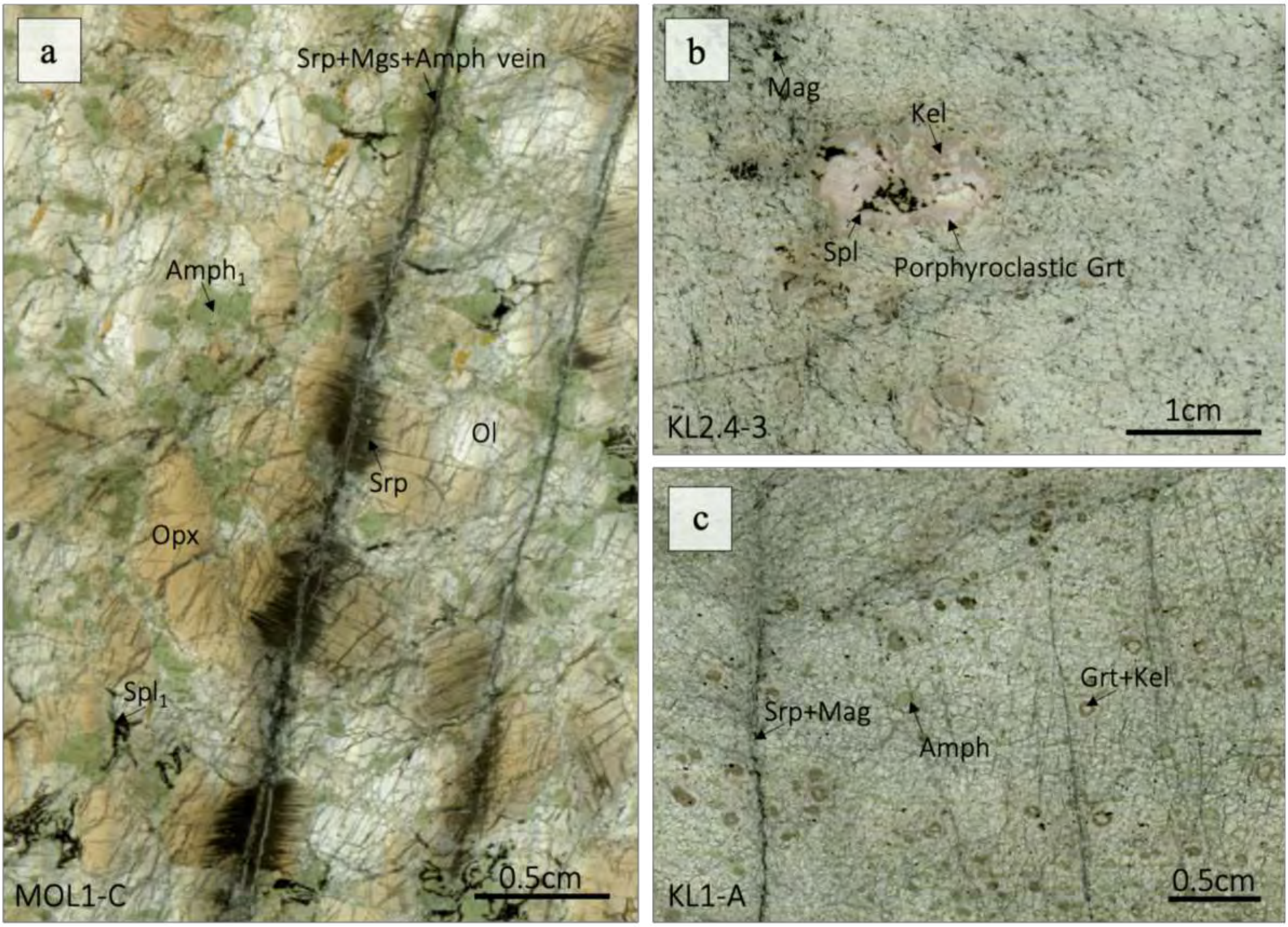
a
Srp+Mgs+Amph vein
Amph1
Ol
Srp
Opx
Spl1
MOL1-C
0.5cm
b
Mag
Kel
Spl
Porphyroclastic Grt
KL2.4-3
1cm
c
Srp+Mag
Amph
Grt+Kel
KL1-A
0.5cm

Figure5

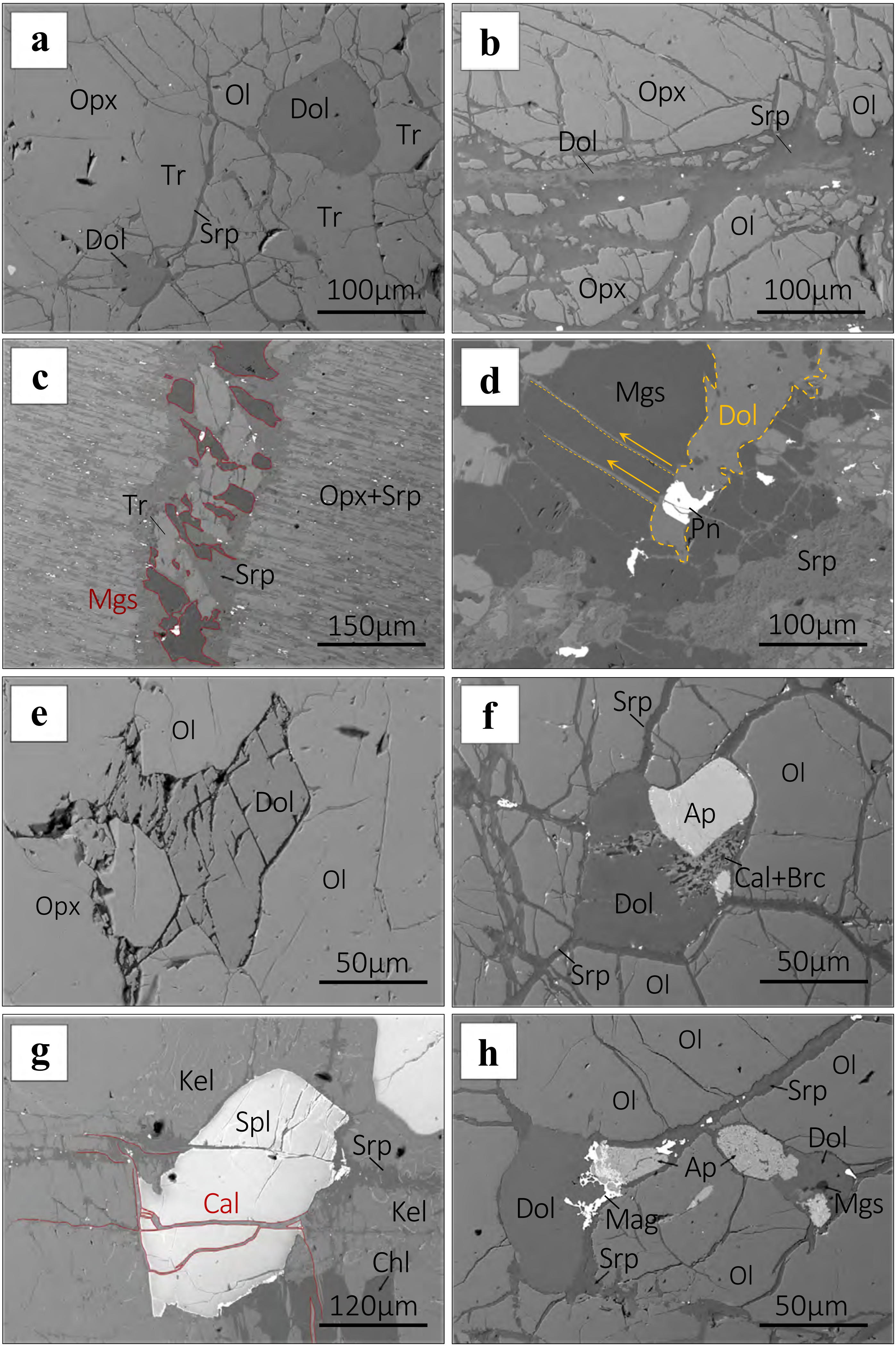
a
Opx
Ol
Dol
Tr
Tr
Tr
Srp
Dol
100μm
b
Opx
Srp
Ol
Dol
Ol
Opx
100μm
c
Tr
Opx+Srp
Srp
Mgs
150μm
d
Mgs
Dol
Pn
Srp
100μm
e
Ol
Dol
Ol
Opx
50μm
f
Srp
Ol
Ap
Cal+Brc
Dol
Srp
Ol
50μm
g
Kel
Spl
Srp
Cal
Kel
Chl
120μm
h
Ol
Ol
Ol
Srp
Dol
Ap
Dol
Mag
Mgs
Srp
Ol
50μm

Figure6

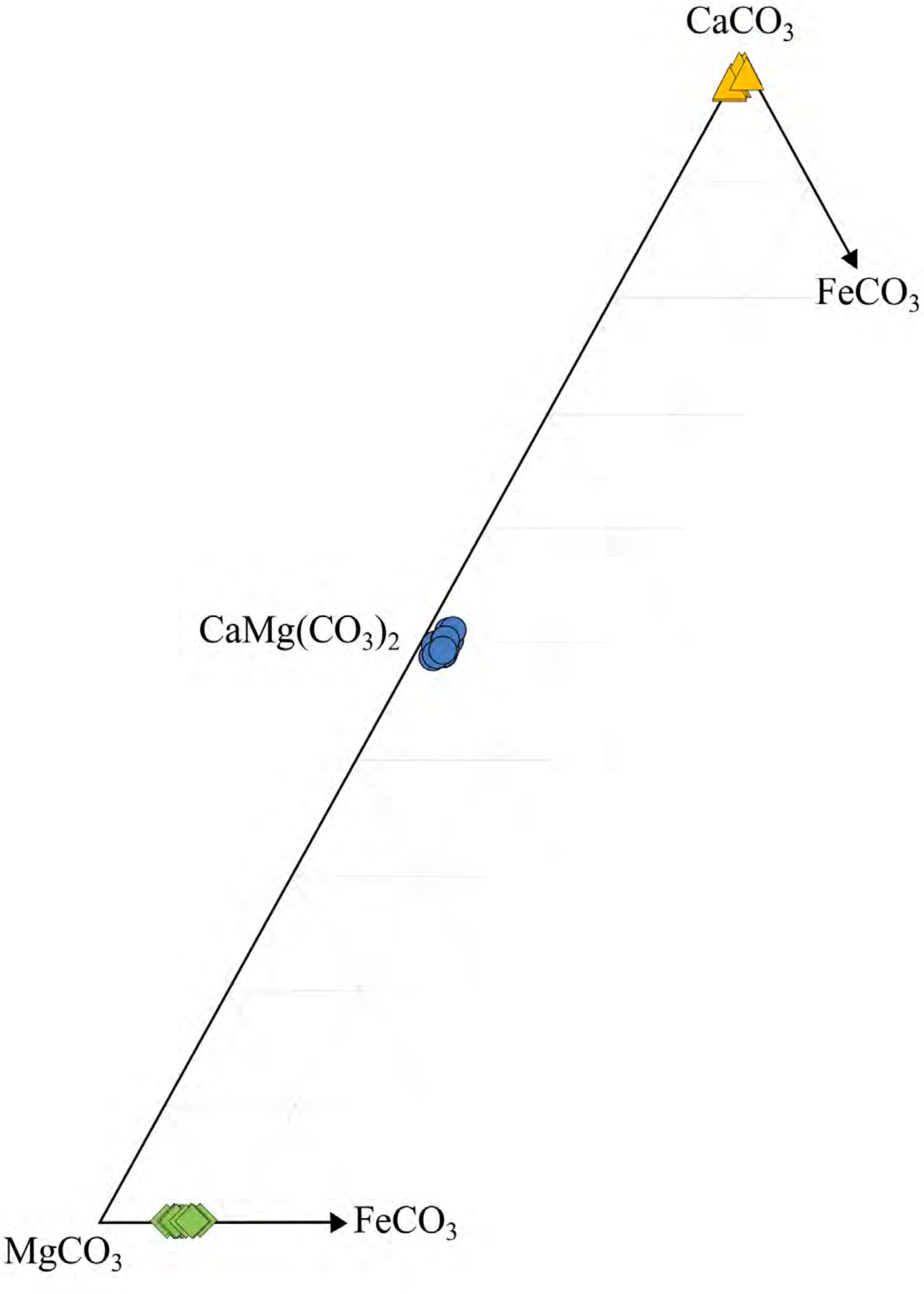

Figure7

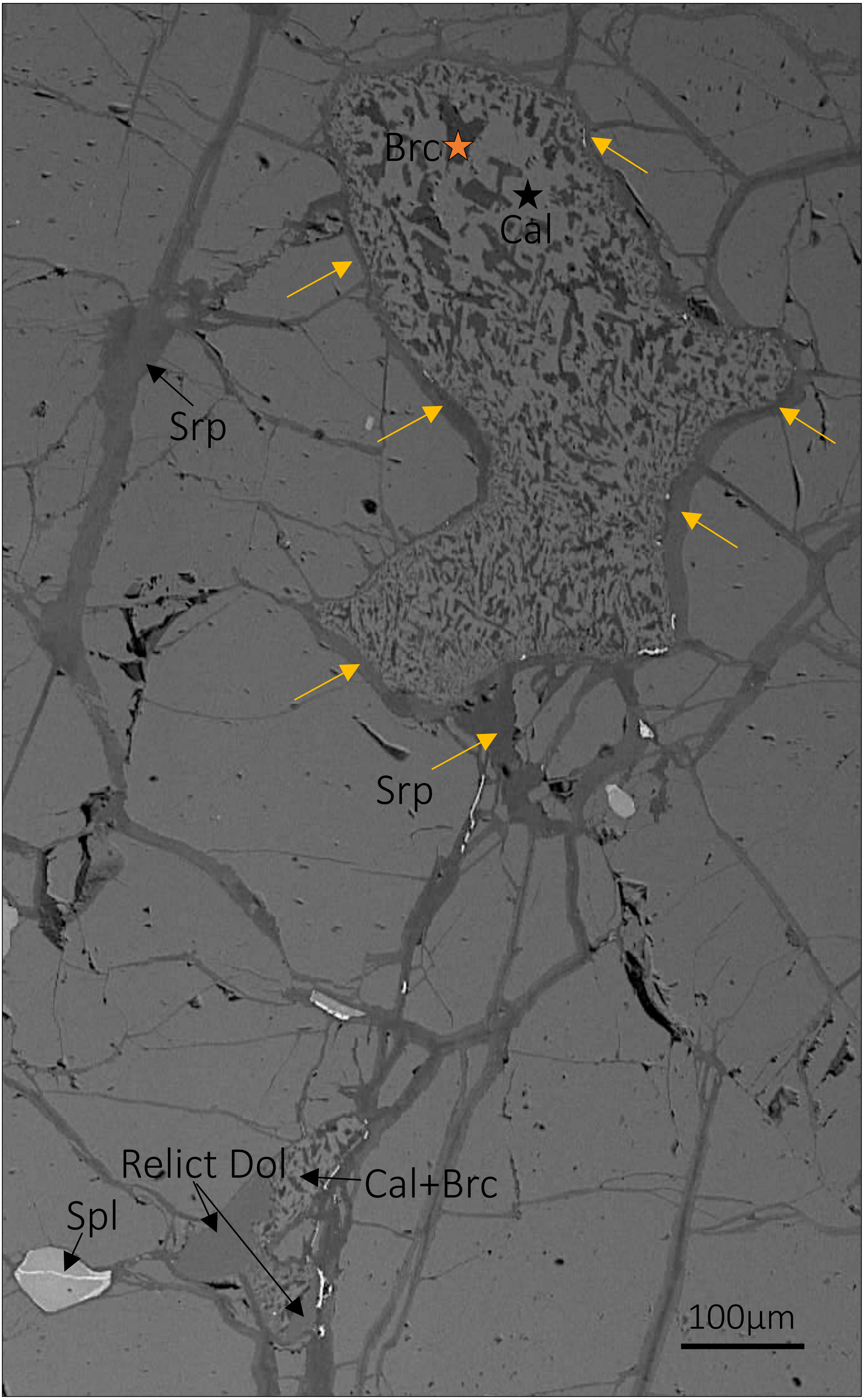

Figure8

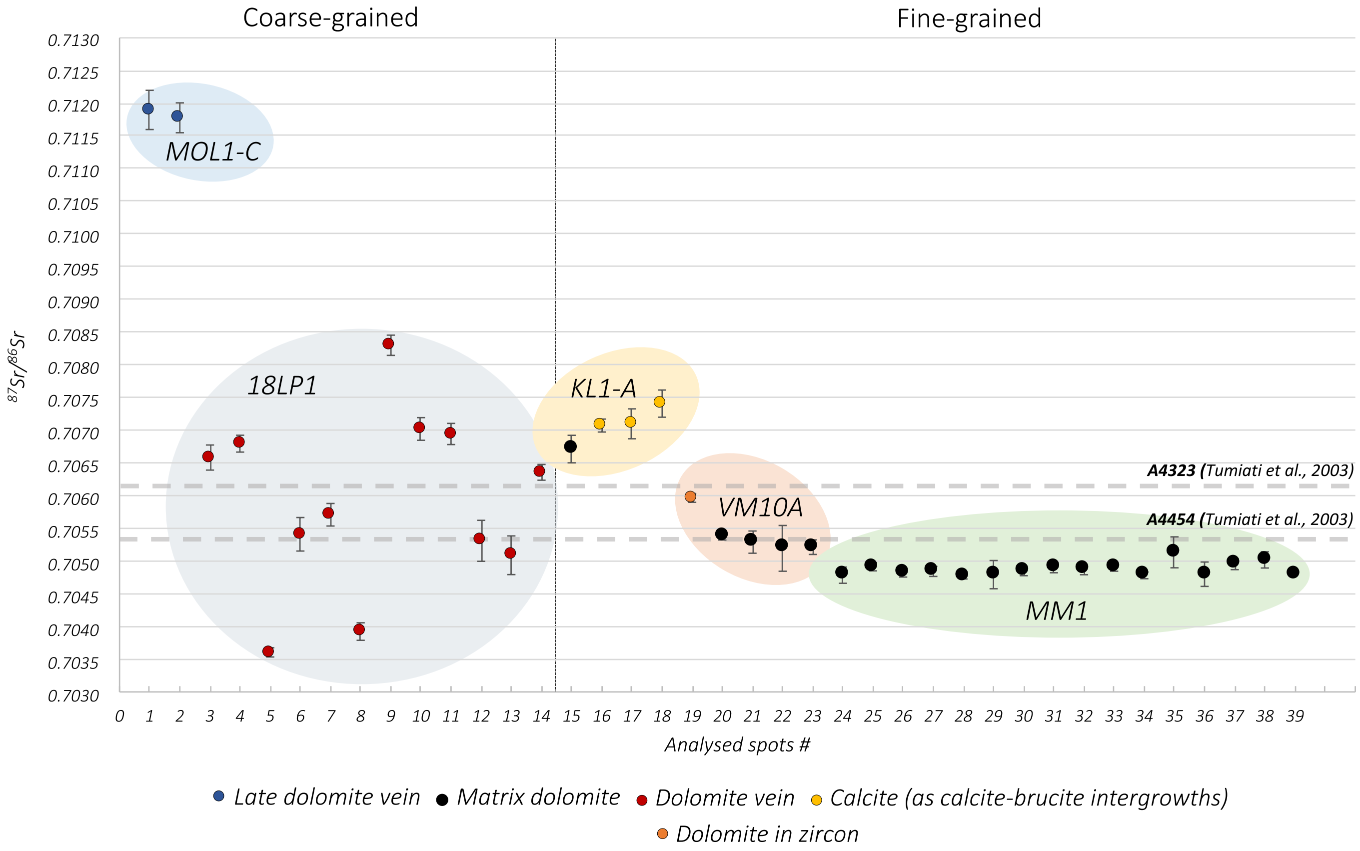
Coarse-grained
Fine-grained
$^{87}Sr/^{86}Sr$
0.7130
0.7125
0.7120
0.7115
0.7110
0.7105
0.7100
0.7095
0.7090
0.7085
0.7080
0.7075
0.7070
0.7065
0.7060
0.7055
0.7050
0.7045
0.7040
0.7035
0.7030
MOL1-C
18LP1
KL1-A
VM10A
MM1
A4323 (Tumiati et al., 2003)
A4454 (Tumiati et al., 2003)
0 1 2 3 4 5 6 7 8 9 10 11 12 13 14 15 16 17 18 19 20 21 22 23 24 25 26 27 28 29 30 31 32 33 34 35 36 37 38 39
Analysed spots #
● Late dolomite vein
● Matrix dolomite
● Dolomite vein
● Calcite (as calcite-brucite intergrowths)
● Dolomite in zircon

Figure9

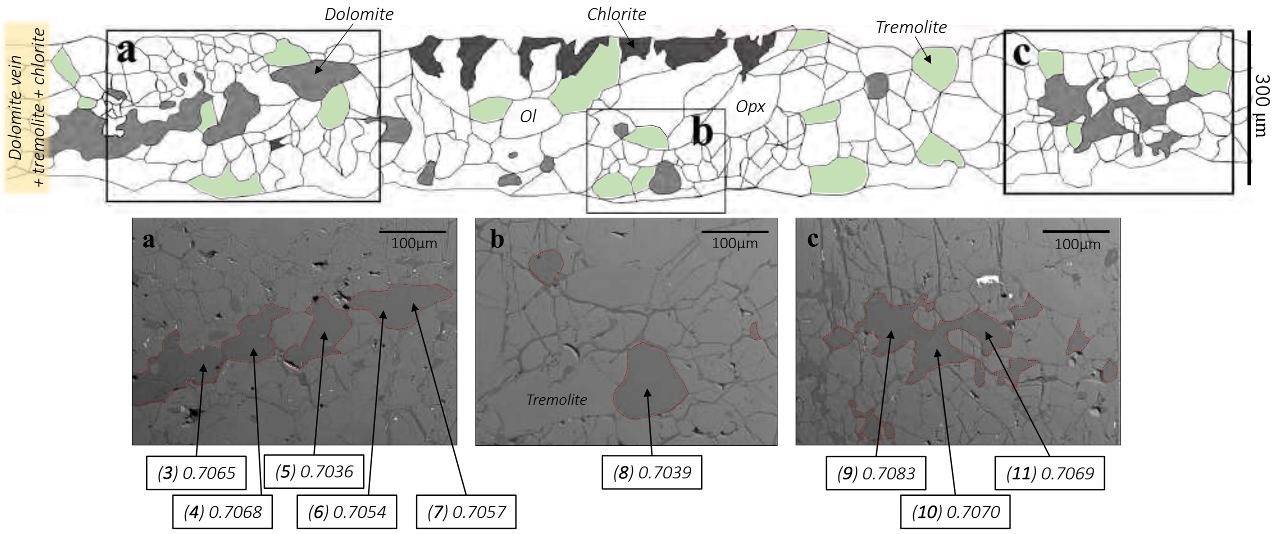
Dolomite vein
+ tremolite + chlorite
Dolomite
Chlorite
Tremolite
Ol
Opx
a
b
c
300 µm
100µm
Tremolite
(3) 0.7065
(4) 0.7068
(5) 0.7036
(6) 0.7054
(7) 0.7057
(8) 0.7039
(9) 0.7083
(10) 0.7070
(11) 0.7069

Figure10

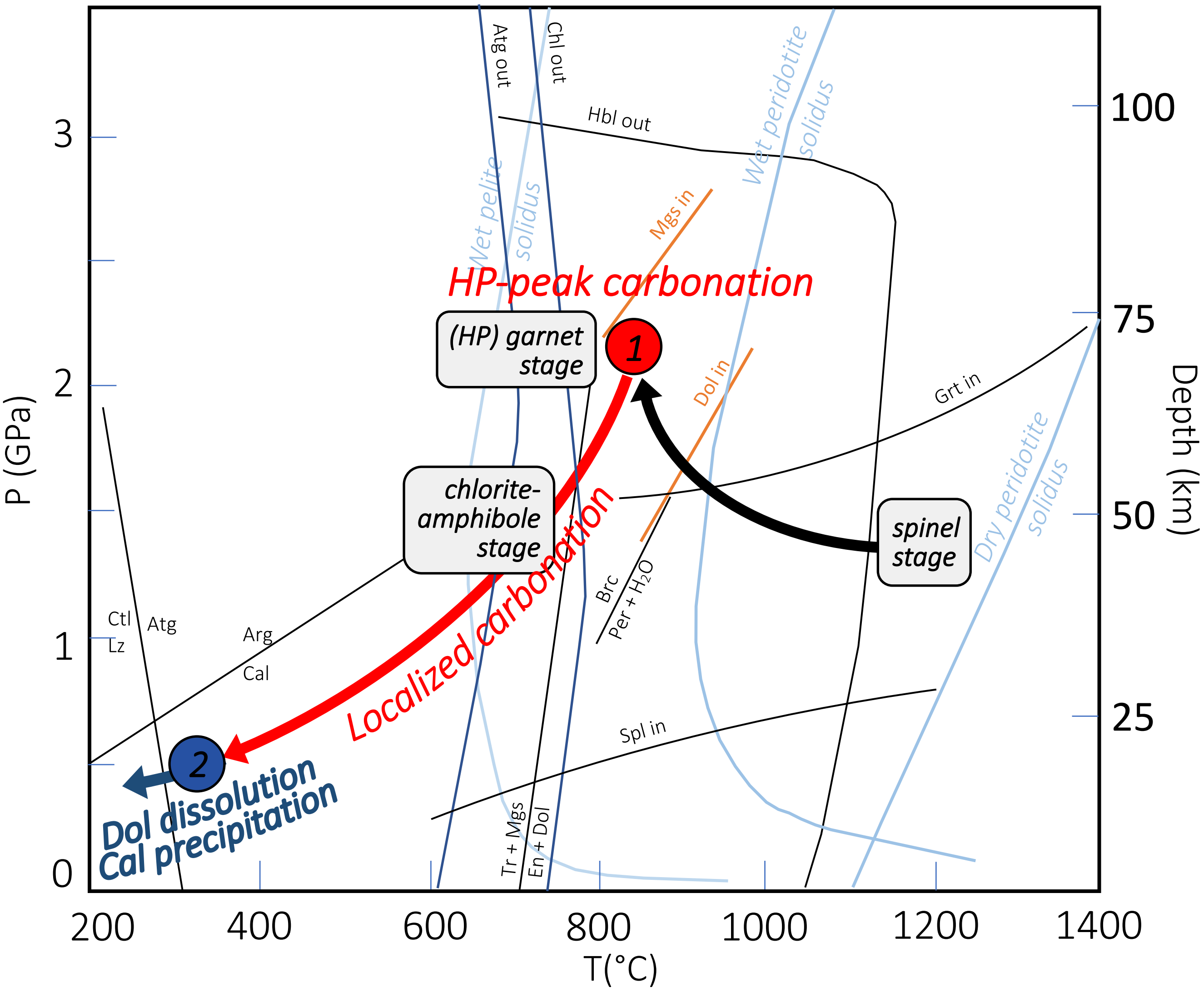
HP-peak carbonation
(HP) garnet stage
1
chlorite-amphibole stage
spinel stage
Localized carbonation
2
Dol dissolution
Cal precipitation
Atg out
Chl out
Hbl out
Wet pelite solidus
Wet peridotite solidus
Dry peridotite solidus
Mgs in
Dol in
Grt in
Spl in
Brc
Per + H_2O
Tr + Mgs
En + Dol
Ctl
Lz
Atg
Arg
Cal
P (GPa)
0
1
2
3
T(°C)
200
400
600
800
1000
1200
1400
Depth (km)
25
50
75
100

Figure11

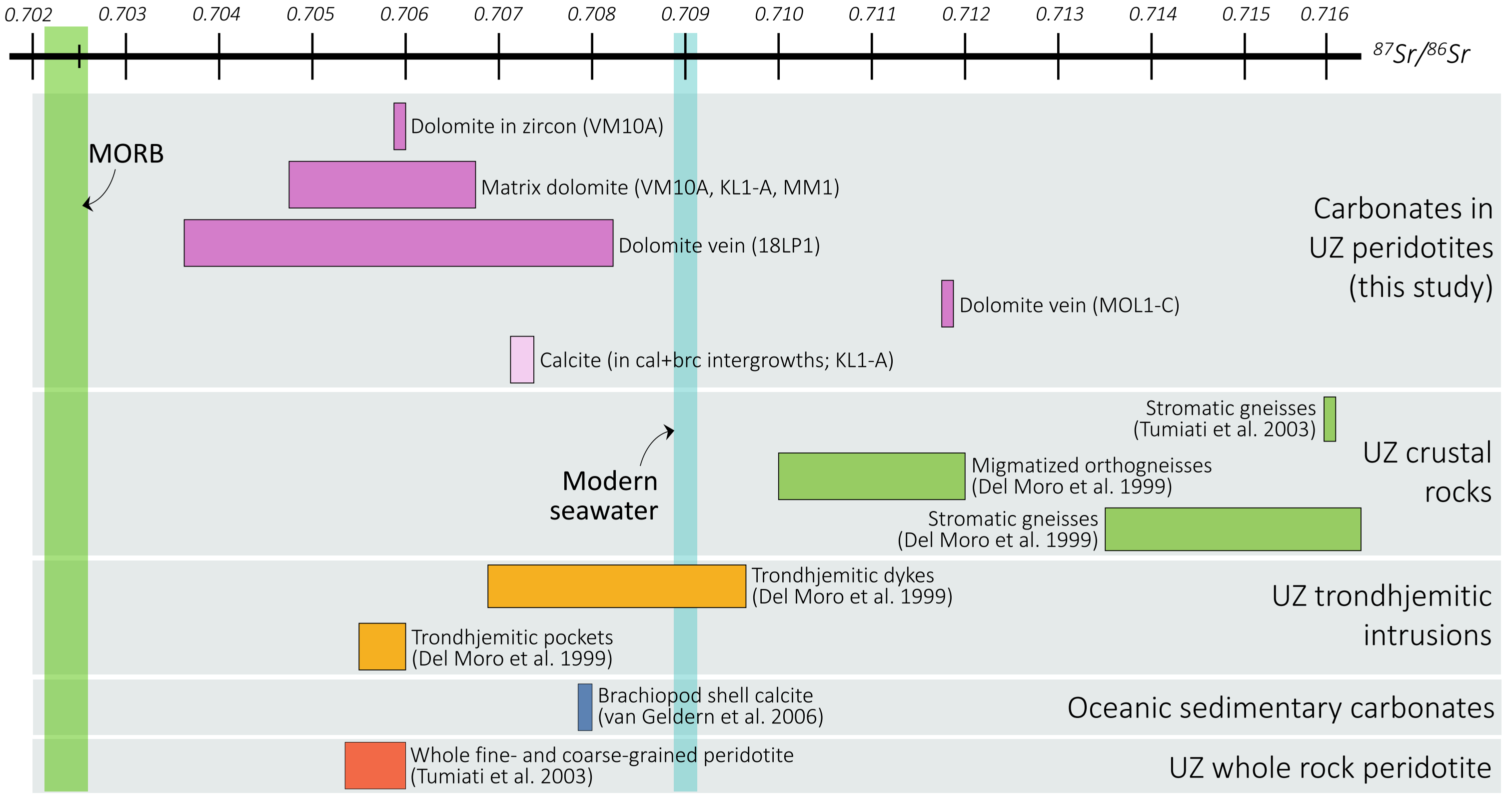

0.702
0.703
0.704
0.705
0.706
0.707
0.708
0.709
0.710
0.711
0.712
0.713
0.714
0.715
0.716
$^{87}Sr/^{86}Sr$
MORB
Dolomite in zircon (VM10A)
Matrix dolomite (VM10A, KL1-A, MM1)
Dolomite vein (18LP1)
Dolomite vein (MOL1-C)
Calcite (in cal+brc intergrowths; KL1-A)
Carbonates in UZ peridotites (this study)
Stromatic gneisses (Tumiati et al. 2003)
Migmatized orthogneisses (Del Moro et al. 1999)
Stromatic gneisses (Del Moro et al. 1999)
Modern seawater
UZ crustal rocks
Trondhjemitic dykes (Del Moro et al. 1999)
Trondhjemitic pockets (Del Moro et al. 1999)
UZ trondhjemitic intrusions
Brachiopod shell calcite (van Geldern et al. 2006)
Oceanic sedimentary carbonates
Whole fine- and coarse-grained peridotite (Tumiati et al. 2003)
UZ whole rock peridotite

Supplementary Materials - Figures

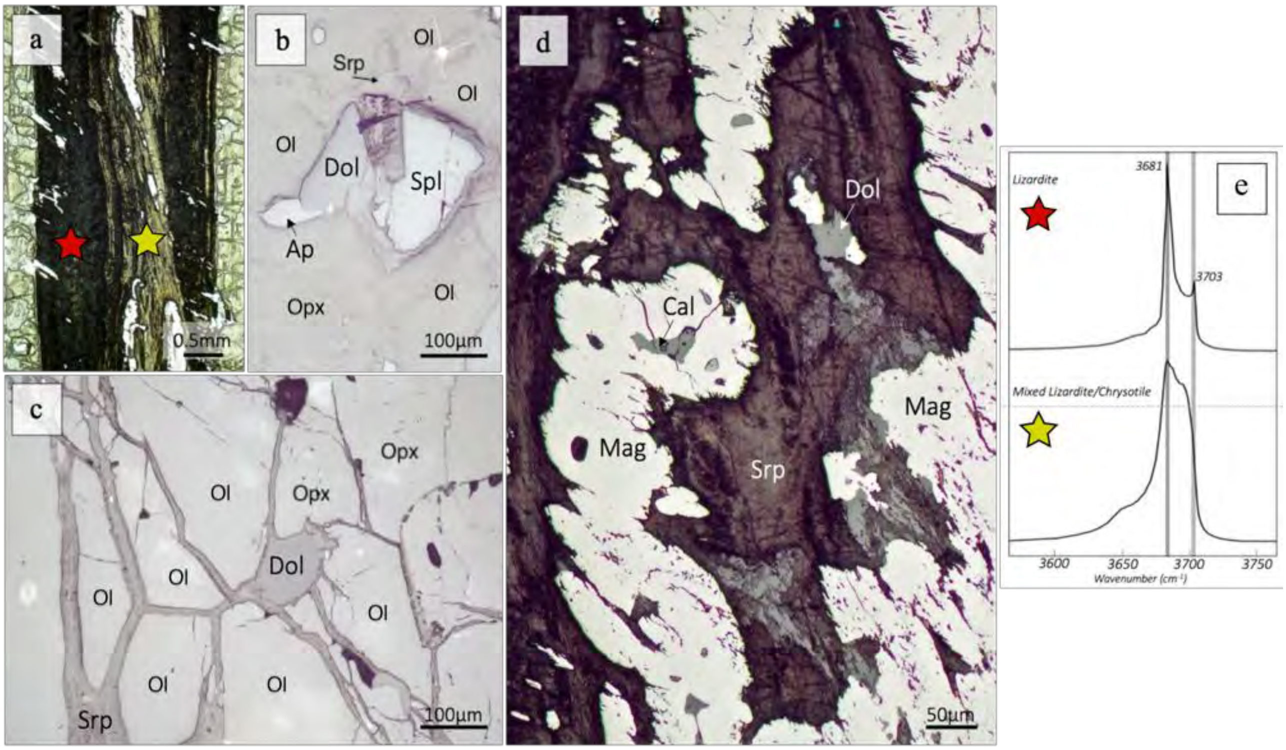

Fig. S1
(a) Zoned serpentine-rich vein cutting the MM1 fine-grained amphibole-chlorite peridotite with its constituting minerals under optical reflected light (b)-(c)-(d). (b) Matrix dolomite associated with Cl-apatite and spinel. (c) Matrix dolomite surrounded by serpentine. (d) Vein core consisting of serpentine + magnetite with calcite and dolomite included; (e) Micro-Raman spectra acquired in the OH region for a composite serpentine vein. Stars represent the analyzed spots. Mineral abbreviations after Whitney and Evans (2010).

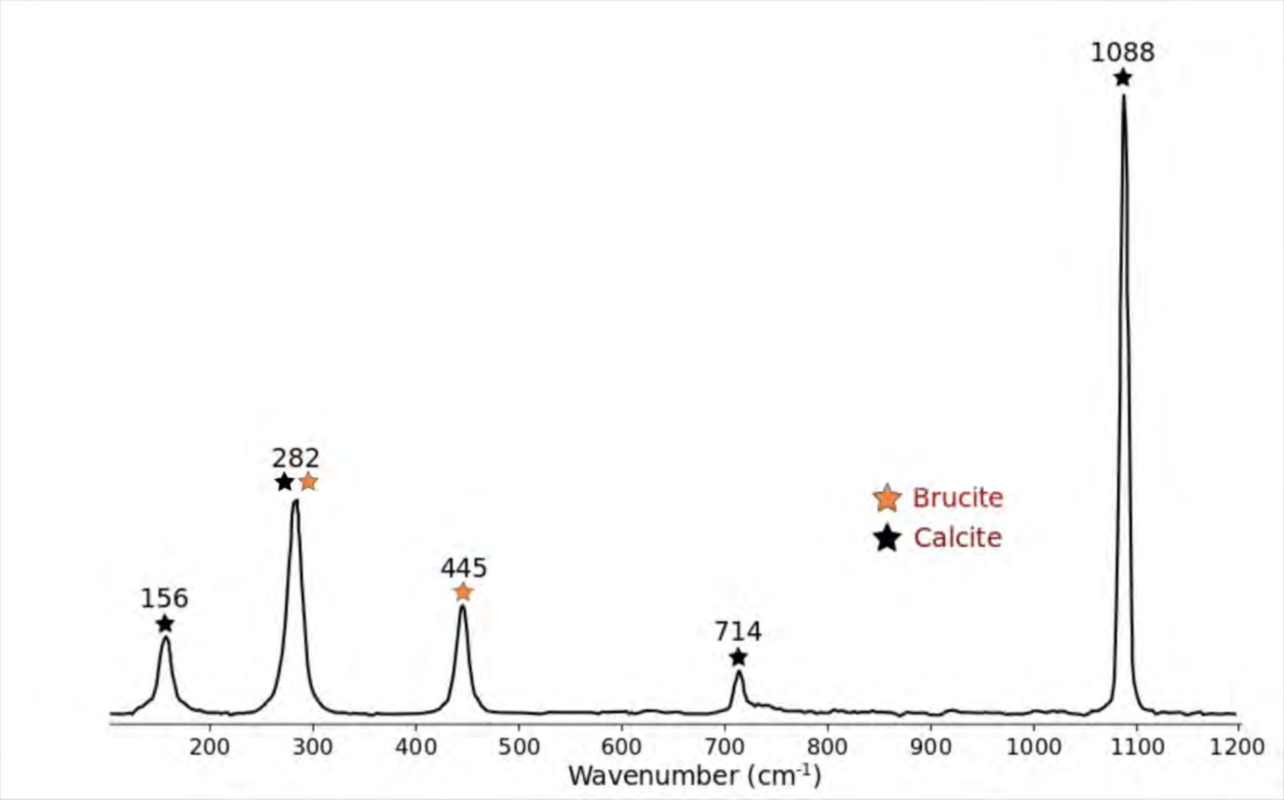

Fig. S2
Micro-Raman spectrum of analyzed calcite and brucite.

Table1. Studied samples from the Ulten Zone.

Sample	Locality	Facies	Texture	Main Assemblage	Carbonates	Serpentinization Grade	Section type	In situ Sr
18LP1	Cima Binasia nearby Lavazze river (as sample LP6; Ionov et al., 2017)	Sp	Coarse	Ol_1 + Opx_1 + Amph + Spl_1 + Cpx_1 + Dol + Chl + Phl + Op	Dolomite veinlet (ca. 300 µm wide) cut by thin serpentine veins with dolomite vein included (ca. 25 µm wide). Abundance: < 1%	Medium	Chip	X
MOL1-C	M.te Ometto	Sp	Coarse	Ol_1 + Opx_1 + Amph + Spl_1 + Mgs + Srp + Chl + Phl + Op	Magnesite vein (ca. 300 µm wide) cut by late dolomite vein (ca. 200 µm long).	Medium	Thick section	X
MM1	Malga Masa Murada (as sample 300B; Morten and Obata, 1990)	Sp	Fine	Ol_2 + Opx_2 + Amph + Spl_2 + Srp + Chl + Dol + Op	Matrix dolomite (50-100 µm; 2% of abundance); dolomite and calcite inclusions (10-50 µm) in magnetite occurring in median line of serpentine vein.	High	Chip	X
KL1-A	Klapfbergalm	Grt	Fine	Ol_2 + Opx_2 + Spl_2 + Grt_2 + Srp +Op	Calcite plus brucite aggregates; matrix dolomite (ca. 50 µm). Abundance : <1 %.	High	Thick section Chip	X
KL2.4-2b **KL2.4-3**	Klapfbergalm	Grt	Porphyroblastic	Ol_2 + Opx_2 + Spl_2 + Grt_2 + Amph + Srp + Dol + Cal + Op	Dolomite inclusion (ca. 70 µm) in a primary spinel,; calcite plus brucite intergrowths (< 1 %).	High	Thick section	
VM10A	Mt.e Hochwart	Gr	Fine	Ol_2 + Opx_2 + Spl_2 + Grt_2	Matrix dolomite (< 1 % of abundance and ca. 60 µm of size) and a mm-sized dolomite inclusion in porphyroblastic zircon.	No	Thick section Chip	X

Mineral abbreviation after Whitney and Evans, (2010)

Table 2. Main representative major elements compositions of minerals measured by EPM.

Mineral	Olivine			Enstatite			Diopside			Amphibole			
M-type sample	C		F	C		F	C	F		C	F	C	
Generation	I	II	I	I	II	II	I	II					
Comment	m	m	m	m	m	m	m	m	Relic in amph	m	m	In mgs vein	In dol+chl+tr vein
SiO$_2$	40.89	40.92	40.80	55.96	56.30	56.94	53.84	54.33	54.00	46.76	45.51	57.26	57.43
Al$_2$O$_3$	bdl	bdl	bdl	2.80	2.51	1.40	1.41	1.27	1.01	10.88	12.01	1.32	0.91
MgO	49.72	49.04	49.23	33.80	33.84	34.61	17.01	17.22	17.47	19.20	18.33	23.20	23.40
CaO	bdl	bdl	bdl	0.27	0.32	0.18	24.78	24.83	24.23	12.06	12.37	12.86	12.92
K$_2$O	bdl	bdl	bdl	bdl	bdl	0.01	bdl	bdl	bdl	0.15	0.55	bdl	bdl
TiO$_2$	bdl	bdl	bdl	bdl	bdl	b~~b~~dl	0.05	bdl	0.12	0.21	0.48	bdl	bdl
FeO	9.57	9.51	9.37	6.33	6.40	6.29	1.56	1.81	1.70	3.07	2.81	2.09	1.70
MnO	0.14	0.15	0.12	0.19	0.11	0.15	0.07	0.06	bdl	b~~b~~dl	bdl	0.10	bdl
Cr$_2$O$_3$	bdl	bdl	bdl	0.26	0.17	0.18	0.38	0.25	0.29	0.85	1.67	0.16	0.26
Na$_2$O	bdl	bdl	bdl	bdl	bdl	b~~b~~dl	0.22	0.22	0.23	2.39	1.95	0.37	0.19
NiO	0.41	0.37	0.40	bdl	0.11	0.02	bdl	bdl	bdl	bdl	bdl	0.06	0.07
Sum	100.72	100.06	99.95	99.70	99.81	99.76	99.58	100.18	99.05	95.57	95.68	97.36	96.95
Si	1.00~~0.995~~	1.00~~2~~	1.00~~0.997~~	1.94~~37~~	1.954~~7~~	1.95~~3~~	1.97~~66~~	1.97~~1~~	1.98~~76~~	6.64~~2~~	6.51~~3~~	7.82~~18~~	7.88~~0~~
Ti							0.00~~1~~	0.00~~2~~	0.00~~3~~		0.05~~1~~		
Al				0.11~~4~~				0.05~~4~~	0.04~~4~~	1.36~~58~~	2.03~~26~~	1.82~~2~~	0.15~~47~~
Cr				0.01~~07~~	0.01~~05~~	0.01~~05~~	0.01~~1~~	0.01~~07~~	0.01~~08~~	0.10~~095~~	0.19~~89~~	0.02~~17~~	0.03~~28~~
Fe^{3+}	0.00~~0~~	0.0~~0~~0	0.0~~0~~0	0.00~~0~~		0.00~~0~~	0.00~~0~~	0.00~~0~~	0.00~~0~~	0.34~~4~~	0.28~~76~~	0.22~~2~~	0.11~~07~~
Fe^{2+}	0.20~~195~~	0.20~~195~~	1.90~~898~~	0.18~~3~~	0.19~~85~~	0.18~~2~~	0.05~~48~~	0.06~~55~~	0.05~~2~~	0.02~~0~~	0.06~~1~~	0.07~~16~~	0.09~~88~~
Mn	0.00~~3~~	0.00~~3~~	0.00~~3~~	0.01~~06~~	0.00~~3~~	0.00~~4~~	0.00~~2~~	0.00~~2~~				0.01~~1~~	
Mg	1.80~~4~~	1.79~~0~~	1.81~~05~~	1.74~~4~~	1.74~~4~~	1.78~~2~~	0.93~~26~~	0.93~~1~~	0.95~~3~~	4.07~~66~~	3.91~~1~~	4.07~~66~~	4.79~~87~~
Ca				0.01~~0~~	0.01~~2~~	0.01~~06~~	0.97~~69~~	0.97~~65~~	0.95~~0~~	1.84~~36~~	1.90~~897~~	1.84~~36~~	1.90~~899~~
Sum	3.01~~05~~	3.00~~3~~	3.00~~4~~	4.01~~09~~	4.01~~07~~	4.00~~3~~	4.01~~09~~	4.01~~07~~	4.00~~3~~	10.55~~47~~	10.56~~4~~	10.01~~05~~	10.00
Mg#	0.90	0.90	0.90	0.91	0.90	0.91	0.95	0.95	0.95	1.00	0.98	1.00	0.96

Olivine, enstatite and diopside generations are labeled I and II based on their composition and texture (see text for details); *C* coarse grained; *F* fine grained; *m* mineral in the matrix; *P* porphyroclast; *In P-grt* included in a porphyroblastic garnet; *mesh* mesh structure; *Bdl* below detection limit.

Formatted: Font: 6 pt

Formatted: Font: 6 pt

Formatted: Font: 6 pt

Formatted: Font: 6 pt

Table2. Continued

Mineral	Pyrope		Cr-Spinel				Lizardite			Chlorite		Phlogopite		Apatite
M-type sample	F		C		F		C	F		C	F	C		F
Generation	I	II	I	II	I	II								
Comment	P	m	m	m	In P-grt	m	vein	mesh	vein	In dol+chl+tr vein	m	m	m	m
SiO_2	41.98	41.82	bdl	0.08	bdl	0.052	41.25	40.02	42.05	30.38	29.85	40.19	37.04	bdl
Al_2O_3	22..6	22.12	45.43	26.47	30.67	37.73	0.34	0.49	0.13	19.08	20.04	14.63	15.07	-
MgO	19.03	18.63	16.13	8.95	9.46	13.93	40.41	39.89	39.53	31.65	32.16	25.53	28.32	bdl
CaO	5.38	5.63	-	-	-	-	bdl	bdl	bdl	0.04	bdl	bdl	bdl	53.45
K_2O	-	-	-	-	-	-	bdl	bdl	bdl	-	Bdl	8.35	5.22	-
TiO_2	bdl	bdl	-	-	0.17	bdl	bdl	bdl	bdl	0.06	0.03	0.21	0.13	-
FeO	9.25	9.70	14.80	24.76	21.24	16.33	2.90	3.72	2.02	2.55	2.22	3.45	5.03	0.41
MnO	0.47	0.63	0.21	0.48	0.49	0.29	bdl	0.12	bdl	bdl	bdl	bdl	0.05	bdl
Cr_2O_3	1.44	1.45	23.09	37.02	35.76	31.01	bdl	bdl	bdl	1.39	1.06	0.76	1.14	-
Na_2O	-	-	-	-	-	-	bdl	bdl	bdl	bdl	bdl	0.13	0.04	bdl
NiO	-	-	0.10	-	bdl	bdl	bdl	-	bdl	0.15	0.17	0.17	0.53	-
Cl	-	-	-	-	-	-	-	0.06	0.06	-			-	5.57
P2O5														39.57
Sum	100.27	99.73	99.80	97.85	97.86	99.35	84.94	84.43	83.83	85.42	85.60	93.45	92.57	99.21
Si	2.99	3.01	0.00	0.00	0.00	0.00	6.23	6.13	6.38	2.92	2.85	2.87	2.67	
Ti				0.00	0.00	0.00				0.00	0.00	0,01	0.01	
Al(IV)	0.01	0.00					1.~~,~~77	1.87	1.62	2.08	2.15	2.13	2.33	
Al(VI)	1.90	1.87	1.48	0.99	1.12	1.29				0.08	0.11	0.21		
Cr	0.08	0.08	0.51	0.93	0.87	0.71				0.11	0.08	0.~~,~~03	0.106	
Fe^{3+}	0.02	0.05	0.00	0.00	0.00	0.00								
Fe^{2+}	0.53	0.54	0.34	0.66	0.55	0.40	0.04	0.05	0.03	0.20	0.18	0.21	0.30	0.06
Mn	0.03	0.04	0.00	0.01	0.01	0.01		0.02						
Mg	2.02	1.99	0.67	0.43	0.44	0.60	9.09	9.10	8.94	4.53	4.58	2.72	3.04	
Ca	0.41	0.44								0.00	0.00			10.18
Cl								0.016	0.01					1.68
P														5.97
Sum	8.00	8.00	3.00	3.00	3.00	3.00	15.76~~3~~	15.864	15.63~~29~~	9.95	10.00	7.90	7.93	17.90
Mg#	0.79	0.78	0.66	0.43	0.44	0.60	0.96	0.95	0.97	0.96	0.96	0.96	0.90	

Table3. Representative EPM~~A~~ analyses of carbonate minerals. Values reported in wt.%. CO_2 reported to 100 for elements recalculations.

Sample	**18LP1**				**MOL1-C**				**MM1**							**VM10A**	
Type	Coarse				Coarse				Fine							Fine	
Mineral	Dol		Dol		Dol		Mgs		Dol		Dol		Dol		Dol	Dol	
Comment	Vein		In opx		Vein w/mgs		Vein		In liz vein		Matrix		In spl		In mag	Matrix	
n	16	2σ	2	2σ	7	2σ	23	2σ	11	2σ	24	2σ	8	2σ	1	42	2σ
MgO	20.65	0.26	20.79	0,09	20.48	0.16	42.45	1.61	20.36	0.45	20.30	0.27	20.06	0.35	20.58	20.29	0.15
CaO	29.58	0.27	29.61	0,12	29.18	0.48	0.18	0.04	29.47	0.10	29.26	0.32	29.19	0.29	29.87	29.42	0.33
MnO	0.06	0.12	0.08	0.11	0.43	0.38	0.23	0.06	0.03	0.06	0.03	0.~~,~~07	0.02	0.05	0.27	0.04	0.00
FeO	1.26	0.15	1.21	0.10	1.31	0.39	5.68	2.10	1.24	0.07	1.34	0.~~,~~09	1.44	0.06	1.96	1.47	0.01
SrO	0.01	0.04	bdl~~0.00~~	~~0.00~~	0.09	0.12	bdl~~0.00~~	~~0.00~~	0.13	0.11	0.~~,~~14	0.~~,~~12	0.20	0.09	bdl ~~0.00~~	0.05	0.02
CO_2	48.44	0.27	48.33	0.22	48.51	0.39	51.46	0.71	48.76	0.34	48.92	0.35	49.11	0.41	47.32	48.73	0.12
Sum	100.00	-	100.00	-	100.00	-	100.00	-	100.00	-	100.00	-	100.00	-	100.00	100.00	-
~~**Mg**~~	~~0.97~~	~~0.01~~	~~0.97~~	~~0,00~~	~~0.96~~	~~0.01~~	~~1.85~~	~~0.05~~	~~0.96~~	~~0.01~~	~~0.96~~	~~0.01~~	~~0.96~~	~~0.01~~	~~0.95~~	~~0.96~~	~~0.01~~
~~**Fe^{2+}**~~	~~0.03~~	~~0.00~~	~~0.03~~	~~0,00~~	~~0.03~~	~~0.01~~	~~0.14~~	~~0.05~~	~~0.03~~	~~0.00~~	~~0.04~~	~~0.00~~	~~0.04~~	~~0.00~~	~~0.05~~	~~0.04~~	~~0.00~~
~~**Mn**~~	~~0.00~~	~~0.00~~	~~0.00~~	~~0,00~~	~~0.01~~	~~0.01~~	~~0.01~~	~~0.00~~	~~0.00~~	~~0.00~~	~~0.00~~	~~0,00~~	~~0.00~~	~~0.00~~	~~0.01~~	~~0.00~~	~~0.00~~
~~**Ca**~~	~~1.00~~	~~0.01~~	~~0.99~~	~~0.00~~	~~0.99~~	~~0.02~~	~~0.01~~	~~0.00~~	~~1.00~~	~~0.01~~	~~1.00~~	~~0,01~~	~~1.00~~	~~0.01~~	~~0.99~~	~~1.00~~	~~0.01~~
~~**Sr**~~	~~0.00~~	~~0.00~~	~~0.00~~	~~0.00~~	~~bdl~~		~~bdl~~	~~0.00~~	~~0.00~~	~~0.00~~	~~0.00~~	~~0,00~~	~~0,00~~	~~0.00~~	~~0.00~~	~~0.00~~	~~0.00~~
~~**C**~~	~~2.00~~	~~0.00~~	~~2.00~~	~~0.00~~	~~2.00~~	~~0.00~~	~~2.00~~	~~0.00~~	~~2.00~~	~~0.00~~	~~2.00~~	~~0,00~~	~~2.00~~	~~0.00~~	~~2.00~~	~~2.00~~	~~0.00~~
~~**Tot**~~	~~4.00~~	~~-~~	~~4.00~~	~~-~~	~~4.00~~	~~-~~	~~4.00~~	~~-~~	~~4.00~~	~~-~~	~~4.00~~	~~-~~	~~4.00~~	~~-~~	~~4.00~~	~~4.00~~	~~-~~
$CaCO_3$	49.84	0.46	49.73	0.01	49.38	0.86	0.28	0.06	50.07	0.54	49.89	0.51	50.03	0.58	49.58	49.99	0.53
$MgCO_3$	48.41	0.47	48.58	0.01	48.23	0.48	92.47	2.73	48.12	0.64	48.16	0.54	47.83	0.54	47.53	47.97	0.57
$MnCO_3$	0.08	0.15	0.10	0.14	0.58	0.50	0.28	0.08	0.04	0.08	0.05	0.09	0.03	0.07	0.~~,~~35	0.05	0.00
$FeCO_3$	1.66	0.20	1.58	0.14	1.73	0.51	6.96	2.66	1.64	0.10	1.78	0.11	1.92	0.08	2.54	1.95	0.02
$SrCO_3$	0.01	0.04	0.00	0.00	0.08	0.11	0.00	0.00	0.12	0.10	0.12	0.11	0.18	0.08	0.00	0.05	0.03
Mg/(Mg+Ca)	0.49	0.00	0.49	0.00	0.49	0.01	1.00	0.00	0.49	0.01	0.49	0.01	0.49	0.01	0.49	0.49	0.01

bdl Below detection limit, *w/cal+brc* associated with cal+brc intergrowths

Formatted: Font: Not Bold

Formatted: Font: Not Bold

Formatted: Font: Not Bold

Formatted: Font: Not Bold

Formatted: Font: Not Bold

Formatted: Font: Not Bold

Table3. Continued.

Sample	**KL1-A**						**KL2.4-2b**						**KL2.4-3**		**KL1.6**	
Type	Fine						Porph-fine						Porph-fine		fine	
Mineral	Dol		Dol		Cal		Dol		Dol		Cal		Cal		Dol	
Comment	Matrix		w/cal+brc		cal+brc		In spl		In spl, w/cal+brc		cal+brc pol.ag.		In spl (in grt)		vein	
n	22	2σ	6	2σ	4	2σ	4	2σ	9	2σ	2	2σ	2	2σ	30	2σ
Wt%																
MgO	20.51	0.23	20.05	0.08	0.33	0.30	20.01	0.30	20.13	1.20	0.38	0.11	0.00	0.00	19.58	0.44
CaO	29.30	0.20	28.97	0.22	54.33	0.37	29.17	0.16	29.82	1.40	49.48	0.43	57.19	0.08	29.74	0.32
MnO	0.11	0.27	0.02	0.06	~~0.00~~bdl	~~0.00~~	0.05	0.07	0.02	0.04	0.03	0.04	bdl~~0.00~~	~~0.00~~	0.04	0.09
FeO	1.52	0.12	1.63	0.06	bdl~~0.00~~	~~0.00~~	1.60	0.08	1.75	0.46	1.41	0.33	0.41	0.15	1.43	0.18
SrO	0.03	0.07	bdl~~0.00~~	~~0.00~~	0.22	0.05	0.09	0.10	0.05	0.09	0.16	0.22	bdl~~0.00~~	~~0.00~~	0.02	0.05
CO_2	48.53	0.26	49.33	0.22	45.12	0.09	49.08	0.27	48.24	2.22	48.53	0.15	42.40	0.23	49.20	0.50
Sum	100.00	-	100.00	-	100.00	-	100.00	-	100.00	-	100.00	-	100.00	-	100.00	-
~~**Mg**~~	~~0.97~~	~~0.01~~	~~0.96~~	~~0.01~~	~~0.02~~	~~0.02~~	~~0,95~~	~~0.01~~	~~0.95~~	~~0.03~~	~~0.02~~	~~0.01~~	~~0.00~~	~~0.00~~	~~1.09~~	~~0.54~~
~~**Fe^{2+}**~~	~~0.04~~	~~0.00~~	~~0.04~~	~~0.00~~	~~0.00~~	~~0.00~~	~~0,04~~	~~0.00~~	~~0.05~~	~~0.01~~	~~0.04~~	~~0.01~~	~~0.01~~	~~0.00~~	~~0.04~~	~~0.02~~
~~**Mn**~~	~~0.00~~	~~0.01~~	~~0.00~~	~~0.00~~	~~0.00~~	~~0.00~~	~~0,00~~	~~0.00~~	~~0.00~~	~~0.00~~	~~0.00~~	~~0.00~~	~~0.00~~	~~0.00~~	~~0.00~~	~~0.00~~
~~**Ca**~~	~~0.99~~	~~0.00~~	~~1.00~~	~~0.00~~	~~1.98~~	~~0.02~~	~~100~~	~~0.01~~	~~1.01~~	~~0.04~~	~~1.93~~	~~0.01~~	~~1.84~~	~~0.02~~	~~1.18~~	~~0.55~~
~~**Sr**~~	~~0.00~~	~~0.00~~	~~0.00~~	~~0.00~~	~~0.00~~	~~0.00~~	~~0.00~~	~~0.00~~	~~0.00~~	~~0,00~~	~~0.00~~	~~0.00~~	~~0.00~~	~~0.00~~	~~0.00~~	~~0.00~~
~~**C**~~	~~2.00~~	~~0.00~~	~~2.00~~	~~0.00~~	~~2.00~~	~~0.00~~	~~2.00~~	~~0.00~~	~~2.00~~	~~0.00~~	~~2.00~~	~~0.00~~	~~2.07~~	~~0.01~~	~~1.84~~	~~0.55~~
~~**Tot**~~	~~4.00~~	~~-~~	~~4.00~~	~~-~~	~~4.00~~	~~-~~	~~4.00~~	~~-~~	~~4.00~~	~~-~~	~~4.00~~	~~-~~	~~3.93~~	~~-~~	~~4.16~~	~~-~~
$CaCO_3$	49.55	0.22	49.82	0.25	98.93	0.77	49.99	0.45	50.36	1.77	96.59	0.66	99.44	0.20	51.15	0.61
$MgCO_3$	48.27	0.39	47.96	0.27	0.85	0.76	47.72	0.46	47.27	1.50	1.04	0.31	000	0.00	46.86	0.68
$MnCO_3$	0.15	0.37	0.03	0.08	0.00	0.00	0.07	0.10	0.02	0.05	0.04	0.06	000	0.00	0.05	0.12
$FeCO_3$	2.00	0.15	2.18	0.08	0.00	0.00	2.14	0.10	2.29	0.54	2.15	0.51	0.56	0.20	1.92	0.25
$SrCO_3$	0.02	0.06	0.00	0.00	0.22	0.05	0.08	0.10	0.05	0.08	0.16	0.23	0.00	0.00	0.02	0.05
Mg/(Mg+Ca)	0.49	0.00	0.49	0.00	0.01	0.01	0.49	0.00	0.48	0.02	0.01	0.00	0.00	0.00	0.48	0.01

Formatted: Font: Not Bold

Formatted: Font: Not Bold

Formatted: Font: Not Bold

Formatted: Font: Not Bold

Formatted: Font: Not Bold

Formatted: Font: Not Bold

Formatted: Font: Not Bold

Formatted: Font: Not Bold

Table4. ^{87}Sr/^{86}Sr and ^{87}Rb/^{86}Sr isotope ratio measured ~~with~~ by LA-MC-ICP-MS for selected carbonates in Ulten Zone peridotites.

Sample and mineral	#	Microstructure	^{88}Sr (V)	^{87}Rb/^{86}Sr	^{87}Sr/^{86}Sr	2se	Spot Size (µm)
MOL1-C							
Dolomite	1	Vein	0.8	<0.0001	0.71189	0.00030	65
Dolomite	2	Vein	1.3	0.0002	0.71178	0.00023	65
18LP1							
Dolomite	9	Vein	1.4	<0.0001	0.70830	0.00015	100
Dolomite	10	Vein	1.6	<0.0001	0.70702	0.00017	100
Dolomite	11	Vein	1.3	<0.0001	0.70694	0.00016	100
Dolomite	8	Vein	2.4	<0.0001	0.70392	0.00013	90
Dolomite	7	Vein	1.2	<0.0001	0.70571	0.00017	90
Dolomite	6	Vein	0.8	0.0001	0.70541	0.00026	65
Dolomite	5*	Vein	3.0	<0.0001	0.70360	0.00007	65
Dolomite	4	Vein	1.2	0.0003	0.70680	0.00013	65
Dolomite	3*	Vein	1.5	0.0001	0.70658	0.00019	100
Dolomite	12	Vein	0.5	<0.0001	0.70531	0.00031	100
Dolomite	13	Vein	0.7	0.0001	0.70509	0.00030	100
Dolomite	14*$^{+}$	Vein	1.6	<0.0001	0.70636	0.00012	100
VM10A							
Dolomite	23*	Matrix	3.4	<0.0001	0.70521	0.00011	65
Dolomite	22*	Matrix	1.2	<0.0001	0.70519	0.00035	65
Dolomite	20*	Matrix	3.4	<0.0001	0.70539	0.00006	65
Dolomite	21*	Matrix	1.6	<0.0001	0.70529	0.00017	55
Dolomite	19^{+}	In zircon	1.3	0.0011	0.70597	0.00007	55
KL1-A							
Dolomite	15	Matrix	1.2	0.0004	0.70671	0.00021	65
Calcite	16	In cal+brc	2.4	<0.0001	0.70707	0.00021	65
Calcite	17	In cal+brc	08	<0.0001	0.70709	0.00023	65
Calcite	18	In cal+brc	1.1	<0.0001	0.70741	0.00009	65
MM1							
Dolomite	24	Matrix	4.7	<0.0001	0.70486	0.00007	65
Dolomite	25*	Matrix	4.4	<0.0001	0.70489	0.00005	65
Dolomite	26	Matrix	4.6	<0.0001	0.70478	0.00005	65
Dolomite	27	Matrix	4.5	<0.0001	0.70490	0.00008	65
Dolomite	28	Matrix	2.4	<0.0001	0.70502	0.00012	65
Dolomite	29	Matrix	3.3	<0.0001	0.70495	0.00008	65
Dolomite	30	Matrix	3.8	0.0002	0.70491	0.00006	65
Dolomite	31	Matrix	2.0	0.0005	0.70478	0.00012	65
Dolomite	32*	Matrix	2.7	0.0004	0.70484	0.00008	65
Dolomite	33	Matrix	4.8	<0.0001	0.70481	0.00005	65
Dolomite	34*	Matrix	1.3	<0.0001	0.70479	0.00022	65
Dolomite	35	Matrix	4.2	<0.0001	0.70477	0.00005	65
Dolomite	36	Matrix	2.9	0.0005	0.70484	0.00007	65
Dolomite	37*	Matrix	1.7	0.0007	0.70513	0.00024	65
Dolomite	38	Matrix	1.5	0.0004	0.70480	0.00019	65
Dolomite	39	Matrix	3.6	<0.0001	0.70479	0.00006	65

~~Table4. ^{87}Sr/^{86}Sr isotope ratio measured with LA-MC-ICP-MS for selected carbonates in Ulten Zone peridotites.~~ (+) A~~a~~nalyses were collected along lines using the same spot size for spot analyses (i.e. 55 µm).
~~. Sr (ppm) concentrations were recalculated from EPMA analyses. b.d.l. is below detection limit. For (*) samples, Sr and Rb concentrations were analyzed in LA-ICP-MS. Rb concentration is below detection limit if <0.0046 ppm. *n.a.* not analysed;~~ *cal+brc* calcite + brucite intergrowths.

Formatted: Superscript

Formatted: Superscript

Formatted Table

Formatted: Centered

Formatted: English (United States)

Formatted: English (United States)

Supplementary Tables

Table I. Major elements compositions (wt%) of olivine. Formula based on 4 oxyg

Anions	4	4	4	4	4
Cations	3	3	3	3	3
Rock type	F	F	F	F	F
Sample	MM1	MM1	MM1	MM1	MM1
Text. Pos.	m	m	m	m	m
Elemento	MM1_ol1	MM1_ol2	MM1_ol3	MM1_ol5	MM1_ol6
MgO	50.1	49.24	49.54	49.89	49.92
Al_2O_3	bdl	bdl	bdl	bdl	bdl
SiO_2	40.85	40.53	40.66	40.56	40.53
TiO2	bdl	bdl	bdl	bdl	bdl
Cr_2O_3	bdl	bdl	bdl	bdl	bdl
MnO	0.16	0.12	0.12	0.12	0.18
FeO	9.54	9.65	9.52	9.42	9.30
NiO	0.36	0.42	0.34	0.35	0.34
Sum	101.01	100.02	100.18	100.34	100.26
Si	0.99	0.99	0.99	0.99	0.99
Ti					
Al					
Cr					
Fe^{2+}	0.19	0.20	0.19	0.19	0.19
Ni	0.01	0.01	0.01	0.01	0.01
Mn	0.00	0.00	0.00	0.00	0.00
Mg	1.81	1.80	1.81	1.82	1.82
Sum	3.01	3.01	3.01	3.01	3.01
Fo	90.20	89.98	90.16	90.31	90.38
Fa	9.64	9.90	9.72	9.57	9.44
Teph	0.16	0.12	0.12	0.12	0.18
N° Mg	90.35	90.09	90.16	90.42	90.54

F: fine-grained; C: coarse-grained; P: porphyroclastic texture; m: matrix . N° Mg, M